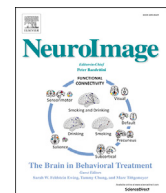




Contents lists available at ScienceDirect

**NeuroImage**  
 journal homepage: [www.elsevier.com/locate/neuroimage](http://www.elsevier.com/locate/neuroimage)



## Neuroimaging of vascular reserve in patients with cerebrovascular diseases

Meher R. Juttukonda <sup>a</sup>, Manus J. Donahue <sup>a,b,c,d,\*</sup>

<sup>a</sup> Department of Radiology and Radiological Sciences, Vanderbilt University Medical Center, Nashville, TN, USA

<sup>b</sup> Department of Neurology, Vanderbilt University Medical Center, Nashville, TN, USA

<sup>c</sup> Department of Psychiatry, Vanderbilt University Medical Center, Nashville, TN, USA

<sup>d</sup> Department of Physics and Astronomy, Vanderbilt University, Nashville, TN, USA

### ARTICLE INFO

**Keywords:**

Cerebrovascular reactivity

Hypercapnia

Cerebral blood flow

Hemodynamics

Stroke

Ischemia

### ABSTRACT

Cerebrovascular reactivity, defined broadly as the ability of brain parenchyma to adjust cerebral blood flow in response to altered metabolic demand or a vasoactive stimulus, is being measured with increasing frequency and may have a use for portending new or recurrent stroke risk in patients with cerebrovascular disease. The purpose of this review is to outline (i) the physiological basis of variations in cerebrovascular reactivity, (ii) available approaches for measuring cerebrovascular reactivity in research and clinical settings, and (iii) clinically-relevant cerebrovascular reactivity findings in the context of patients with cerebrovascular disease, including atherosclerotic arterial steno-occlusion, non-atherosclerotic arterial steno-occlusion, anemia, and aging. Literature references summarizing safety considerations for these procedures and future directions for standardizing protocols and post-processing procedures across centers are presented in the specific context of major unmet needs in the setting of cerebrovascular disease.

### Introduction

Functional neuroimaging methods commonly exploit changes in cerebral blood flow (CBF; ml blood/100 g tissue/minute) as a surrogate marker of neuronal activity. In humans, such studies initially utilized positron emission tomography (PET) and single-photon emission computed tomography (SPECT) radioisotopes, or transcranial Doppler (TCD) to evaluate flow velocity, but have expanded more recently to include noninvasive (e.g., without exogenous contrast administration) blood oxygenation level-dependent (BOLD) and arterial spin labeling (ASL) magnetic resonance imaging (MRI). These methods exploit the phenomena that flow velocity, CBF, and cerebral blood volume (CBV; ml blood/100 g brain) increase locally when healthy brain parenchyma enters a state of increased neuronal activity or metabolic demand, and as such the hemodynamic measures provide surrogates of dynamic brain activity.

When performed concurrently with neuronal stimuli where the cerebral metabolic rate of oxygen ( $\text{CMRO}_2$ ; ml  $\text{O}_2/100 \text{ g tissue}/\text{minute}$ ) increases, hemodynamic changes occur owing to a complex interaction of vasodilatory effects from neurotransmitter-mediated signaling cascades and from byproducts of oxidative metabolism and corresponding changes in pH. Distinguishing the extent to which neuronal or vascular phenomena underlie aberrant functional imaging signals or flow

dysregulation is not straightforward, as many hemodynamic imaging methods have multiple signal sources, but few direct observables.

Alternatively, it is possible to administer largely isometabolic stimuli in which vascular resistance is altered as a result of the vasoactive effects of pharmacological or respiratory stimuli. Such experiments elicit a change in CBF and CBV with a small-to-negligible concurrent change in  $\text{CMRO}_2$  and thus provide a so-called measure of cerebrovascular reactivity (CVR). CVR magnitude, which is most fundamentally quantified as the fractional change in CBF between a baseline and vasodilatory stimulus, has been investigated as a marker of microvascular health in numerous conditions.

The purpose of this review is to summarize (i) the regulation of cerebral blood flow in humans, (ii) the physiological relevance of CVR in the context of healthy and ischemic physiology, (iii) available approaches that can be used in research or clinical settings for externally modulating vascular resistance and eliciting CVR responses, (iv) available neuroimaging techniques for measuring CVR directly and indirectly, (v) imaging parameters and analysis considerations, (vi) relevant literature findings in which these methods are applied specifically to patients with cerebrovascular disease, and (vii) potential future research directions.

Elegant review articles on a subset of topics have been published and should be referred to for additional information. These articles highlight

\* Corresponding author. Vanderbilt University Institute of Imaging Science, 1161 21st Avenue South AAA-3115, Medical Center North, Nashville, TN 37232, USA.  
 E-mail address: [mj.donahue@vanderbilt.edu](mailto:mj.donahue@vanderbilt.edu) (M.J. Donahue).

applications of novel noninvasive MRI methods in the setting of cerebrovascular disease (Donahue et al., 2012), along with salient clinical findings (Smeeling et al., 2016) and post-processing concerns (Donahue et al., 2016a); an overview of available methods for manipulating blood gases with respiratory stimuli (Moreton et al., 2016) and breath hold (Urback et al., 2017), along with specific review articles on relevant measurement imaging tools including ASL MRI (Alsop et al., 2015; Telischak et al., 2015), BOLD MRI (Christen et al., 2013; van Zijl et al., 1998), SPECT perfusion (Masdeu and Brass, 1995), PET perfusion (Derdeyn et al., 1999), and TCD (Willie et al., 2011). Here, methodological imaging and stimulus tools are presented with specific attention to benefits and limitations in patients with ischemic cerebrovascular disease.

### The regulation of cerebral blood flow in humans

Oxygen is consumed by the adult brain at an approximate rate of 49 ml O<sub>2</sub>/min, or 3.5 ml O<sub>2</sub>/100 g/min for a typical adult brain of 1400 g (Kennedy and Sokoloff, 1957). Compared with a whole-body oxygen consumption rate of 250 ml O<sub>2</sub>/min (Kennedy and Sokoloff, 1957), the brain consumes a disproportionate fraction of oxygen relative to its size, and the brain is dependent on a continuous supply of oxygen and energy substrate from the blood. Blood is delivered to the brain tissue primarily through the left and right internal carotid arteries (ICAs) and basilar arteries (Fig. 1). The ICAs and basilar artery supply blood to the Circle of Willis (CoW), a circulatory arterial anastomosis, which is central to distributing blood to the anterior and posterior flow territories and also dampening vascular pulsations from high flow velocity blood in cervical vessels (Vrselja et al., 2014). At the level of the CoW, blood is delivered to anterior bilateral regions of the anterior cerebral artery (ACA) and middle cerebral artery (MCA), with the posterior cerebral artery (PCA) delivering blood to the posterior flow territories (Purves and Williams, 2001). The ACA flow territory consists of the medial portions of the frontal and parietal lobes, the MCA flow territory consists of the frontal, parietal, and temporal lobes, and the PCA flow territory consists of the

inferior temporal lobe and the occipital lobe. Peak blood flow velocities measured using TCD are largely symmetric between left and right arteries in healthy adults with normal vascular anatomy and non-flow-limiting stenosis, and have been reported to be 65–77 cm/s in ICAs, 92–105 cm/s in MCAs, 57–66 in PCAs, and 74–91 cm/s in the ACAs, and 49–55 cm/s in the basilar artery (Enzmann et al., 1994). Mean values over the cardiac cycle are 37–47 cm/s in ICAs, 59–68 cm/s in MCAs, 36–43 cm/s in PCAs, and 48–56 cm/s in the ACAs, and 34–38 cm/s in the basilar artery (Enzmann et al., 1994). It should be noted that flow velocities quantified from phase contrast magnetic resonance angiography can be 30–40% lower than those reported from TCD using conventional techniques, partly attributable to underestimations in flow velocities in phase contrast angiography due to the parabolic flow profile of blood, cardiac cycle averaging, and lower spatial resolution. Fig. 1 shows major cervical and intracranial blood vessels, along with the approximate flow territories that the major cervical vessels perfuse. It should also be noted that precise flow territories are highly variable between even healthy subjects owing to normal anatomical variations in the CoW (Hendrikse et al., 2005).

MRI-based measurements of bulk blood flow in healthy adults show that approximately 750 ml blood/minute is delivered to the brain tissue through the ICAs and basilar artery, which contribute approximately 80% and 20% of the total blood supply, respectively (Oktar et al., 2006). For typical adult brain weights of 1300–1400 g, this leads to a CBF of 40–60 ml/100 g/min over a healthy range of perfusion pressures (Cipolla, 2009). Disruption of the blood supply, through either steno-occlusion or changes in cardiac output can quickly result in reduced oxygen delivery to tissue and in advanced stages cell death. Oxidative glucose metabolism becomes impaired for CBF values of approximately 25 ml/100 g/min or lower, followed by tissue acidosis and ATP reduction (CBF < 20 ml/100 g/min), irreversible paralysis (CBF < 15 ml/100 g/min) and major shifts in intracellular sodium, potassium, water, and calcium (CBF < 10 ml/100 g/min) (Baron, 2001; Leigh et al., 2017). CBF threshold values are based on early PET literature, approximate, and precise thresholds depend on multiple factors and

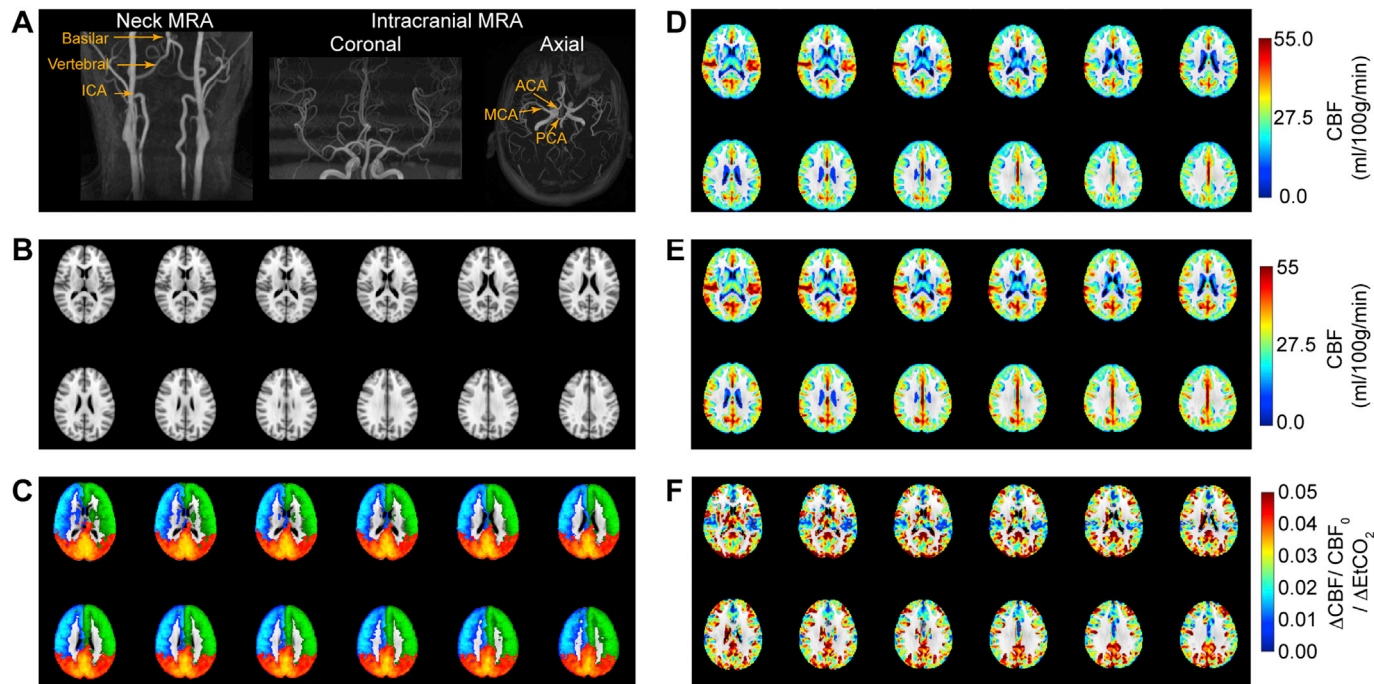


**Fig. 1.** Healthy cerebral blood flow (CBF) and cerebrovascular reactivity (CVR) patterns. (A) Major neck and head vessels as visualized from 3.0 T time-of-flight magnetic resonance angiography. (B) Tissue atlas (Montreal Neurological Institute; 2 mm isotropic) and (C) corresponding flow territories averaged from healthy adults overlaid on the atlas, as quantified from vessel-encoded arterial spin labeling MRI (red = basilar artery; green = left ICA; blue = right ICA). (D) Normocapnic normoxic CBF, (E) Hypercapnic (5% CO<sub>2</sub>) normoxic CBF, and corresponding (F) CVR quantified as the fractional CBF change normalized by the end-tidal change in CO<sub>2</sub> (EtCO<sub>2</sub>) in 10 healthy subjects. CBF was determined using arterial spin labeling and thresholded to show gray matter only, as white matter CBF values are less reliable using ASL at 3.0T. Additional information can be found in (Donahue et al., 2014b).

individual physiology. The intracranial microvasculature and parenchyma contains complex mechanisms for regulating blood delivery through collateral networks and autoregulatory changes in CBV, which can contain insights as to how well brain tissue is compensating for large vessel disease.

Blood flow to the brain is tightly regulated to maintain adequate levels of oxygen delivery to tissue (Guyton and Hall, 2006), and CBF adjusts in responses to changes in cerebral perfusion pressure (CPP) according to,

$$CBF = \frac{CPP}{Cerebrovascular resistance} \quad (1)$$

where CBF is the rate of blood delivery to tissue, CPP is the difference between intra-arterial pressure and venous pressure and is approximately 80 mmHg, but can span a large range (e.g., 60–160 mmHg) and cerebrovascular resistance is governed partly by large vessels (e.g., ICAs and vertebrobasilar arteries), but to a larger extent by smaller arterioles with diameter < 100 μm in a system of segmented vascular resistance. CPP is also frequently considered in terms of mean arterial pressure (MAP) and more commonly measured intracranial pressure (ICP),

$$CPP = MAP - ICP \quad (2)$$

where,

$$MAP = \text{diastolic pressure} + \frac{1}{3}(\text{systolic pressure} - \text{diastolic pressure}) \quad (3)$$

MAP is generally 65–110 mmHg and ICP is 7–15 mmHg supine. As such, the CPP is directly affected by physiological changes that alter MAP or ICP, such as changes in arterial vessel diameter or cardiac output. Vascular resistance can change through the relaxation of smooth muscle that lines arterioles and enables elevated blood delivery to adjust dynamically to meet local energy demands. In this context, flow can also be described by adapting Poiseuille's law:

$$CBF = \frac{CPP \cdot \pi r^4}{8\eta l} \quad (4)$$

where  $r$  is the radius of the vessel,  $l$  is the length of the vessel, and  $\eta$  is the viscosity of blood, generally  $3.5 \times 10^{-3}$  Pa s, and CPP is the cerebral perfusion pressure as defined above. The most relevant conclusion from Eq. (4) for this work is that CBF regulation can occur to the largest degree as a result of changes in CBV, as vessel radius and CBF are related by a power of four. As such, in response to reductions in CPP, CBF can be maintained over a large range through regulation of microvascular vessel diameter, a process termed autoregulation (Cipolla, 2009). A detailed discussion of vessel resistance and velocity as a function of diameter has been elegantly summarized in the literature (Piechnik et al., 2008) and a graphical description of these findings is shown in Fig. 2.

The manner in which microvascular vasodilation occurs in response to reductions in CPP or elevated metabolic demand is governed by cells within the neurovascular unit (Hawkins and Davis, 2005; Kim and Filosa, 2012), which consists of neurons, astrocytes, endothelial cells, myocytes, pericytes, and extracellular matrix components. Detailed reviews of the neurovascular unit and its relevance for regulating CBF have been described in the literature, and these models have been updated to outline the role of cerebral capillaries (Itoh and Suzuki, 2012) and astrocytes (Filosa et al., 2016). Multiple mechanisms relevant to cerebrovascular disease can lead to modulation of CBF and CBV. Hypoxia, or decreased tissue oxygen pressure ( $pO_2$ ) which may occur as a result of either elevated oxygen demand or reduced oxygen supply, will lead to increases in CBF and CBV through either direct mechanisms in which the reduced  $O_2$  is insufficient to maintain smooth muscle contraction or more indirectly by mediating vasodilatory metabolites. Of particular relevance

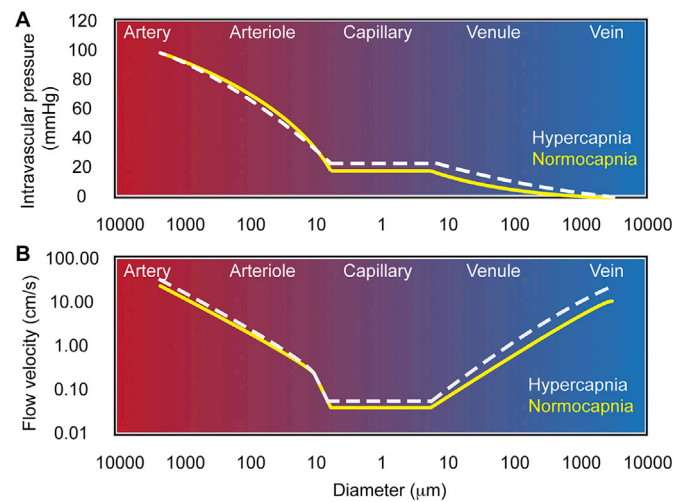


**Fig. 2.** Relationships between vessel diameter and intravascular pressure (A) and flow velocity (B); data are adapted from data summarized in Piechnik et al. (Piechnik et al., 2008), and based on human and animal literature reports of  $\text{PaCO}_2$ -manipulated perfusion over a range of 25–70 mmHg.

to this work is the reversible effect of  $\text{CO}_2$  and hydrogen ions ( $\text{H}^+$ ) on vascular tone. Hypercapnia (e.g., elevated partial pressure of  $\text{CO}_2$ ,  $\text{pCO}_2$ ) and hypcapnia (e.g., reduced  $\text{pCO}_2$ ) elicit vasodilation and vasoconstriction of the cerebral vasculature, respectively, and can be described in the context of dissolved  $\text{CO}_2$  in water:



$\text{CO}_2$  and water form carbonic acid, which is in equilibrium with bicarbonate and hydrogen ions. An increase in blood  $\text{CO}_2$  level will increase carbonic acid formation and ultimately increase  $\text{H}^+$ , thereby reducing pH by definition. *In vivo*, there are multiple processes that provide regulatory control of CBF by altering  $\text{pCO}_2$  and pH, and the precise mechanisms of this regulation have not been fully elucidated. It is generally believed that changes in vascular tone occur most directly as a result of extracellular changes in pH. This is based on seminal work (Kontos et al., 1977) in which pial arteriole dilation in cats was observed during application of CSF with low pH, and this was observed regardless of  $\text{pCO}_2$ , and vasoconstriction was observed when the pH was elevated and independent of  $\text{pCO}_2$ . The caliber of these vessels was also unchanged in response to changes in  $\text{pCO}_2$  only or bicarbonate ions, leading to the conclusion that extracellular fluid pH is the major direct contributor to changes in vascular tone. However, *in situ* work has demonstrated that MCA contraction is possible by reducing  $\text{pCO}_2$  by more than two-fold while maintaining pH, and relaxation is possible upon increasing the  $\text{pCO}_2$  for constant pH (Harder and Madden, 1985). It has also been suggested that pH changes alone are insufficient to fully account for vasodilation, and *in situ* rabbit basilar artery preparations demonstrated that increasing extracellular pH in the absence of  $\text{CO}_2$  changes did not elicit vasoconstriction (Aoyama et al., 1999; Kim et al., 2004). A detailed summary of *in vivo* and *in situ* work on the mechanism of  $\text{pCO}_2$ -induced changes on vascular tone is beyond the scope of this article, however the interested reader is referred to the literature in which these studies, along with their strengths and limitations, have been summarized in detail (Yoon et al., 2012). What is most relevant for the discussion to follow is that (i) reductions in CPP reduce CBF and reductions in vascular resistance increase CBF, (ii) CBF can be modulated by small changes in CBV owing to the sensitive relation between CBF and vessel radius, and (iii) reductions in blood  $\text{CO}_2$  will lead to vasoconstriction and increases in blood  $\text{CO}_2$  will lead to vasodilation. The remainder of this document will focus on mechanisms by which the brain modulates these parameters, as well as abilities to modulate and measure them directly with vascular stimuli

and neuroimaging, respectively.

### Physiological relevance of cerebrovascular reactivity in ischemia

Cerebral ischemia will arise due to reductions in oxygen delivery to tissue, and can occur as a result of reduced oxygen delivery without arterial steno-occlusion (e.g., anemia or generalized hypoxic hypoxia) or decreases in CPP as a result of arterial steno-occlusion. In cases of reduced oxygen delivery for any of the above reasons, vasodilation of pial arterioles will ensue, resulting in a decrease in vascular resistance and increase in flow. In some cases, these tissue-level compensations may be sufficient to ensure the necessary supply of oxygen, but chronic reductions or acute changes in oxygen delivery may cause these vessels to approach their limit for dilation, or exhaust cerebrovascular reserve capacity. When this occurs, this autoregulatory method of compensation is no longer sufficient to maintain adequate oxygen delivery to tissue, and the oxygen extraction fraction (OEF; ratio of oxygen consumed to oxygen delivered) (Powers, 1991) will increase (Fig. 3). These parameters can be expressed by the basic relationship,

$$OEF = \frac{\text{Oxygen consumed}}{\text{Oxygen delivered}} = \frac{CMR_{O_2}}{CBF \cdot Y_a \cdot [Hb]} \quad (6)$$

where  $CMR_{O_2}$  is the cerebral metabolic rate of oxygen (3–4 ml O<sub>2</sub>/100 g/min in healthy tissue), CBF is the cerebral blood flow,  $Y_a$  is the arterial oxygen saturation fraction (96–99% in healthy arterial blood), and [Hb] is the total hemoglobin concentration (Table 1). As can be seen from Eq. (6), when either CBF or oxygen carrying capacity ( $Y_a \cdot [Hb]$ ) reduces, OEF will increase when  $CMR_{O_2}$  is unchanged. As it is believed that  $CMR_{O_2}$  is maintained or reduces only slightly until advanced stages of disease, impairment in oxygen delivery is believed to be the primary contributor to elevated OEF in mild-to-moderate stages of ischemia.

The St. Louis Carotid Occlusion study demonstrated that elevated OEF is an independent predictor of stroke in patients with carotid occlusion (Grubb et al., 1998) with an ipsilateral ischemic stroke rate at two years of 5.3% in 42 patients with normal OEF and 26.5% in 39 patients with increased OEF ( $p = 0.004$ ). However, OEF measurements using similar <sup>15</sup>O PET procedures are limited to specialized centers with on-site cyclotrons. MRI has recently emerged as a noninvasive alternative for obtaining OEF measurements (Fernandez-Seara et al., 2006; Lee et al.,

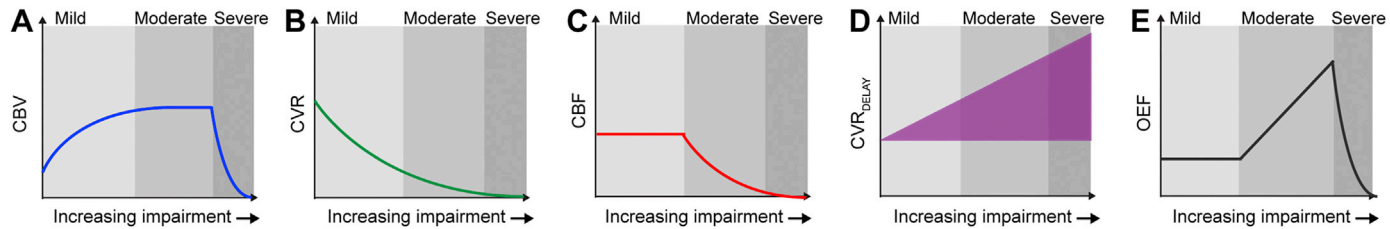


**Fig. 3.** Physiological changes in early stages of cerebrovascular disease. For increasing levels of impairment and cerebral perfusion pressure (CPP) reduction, cerebral hemodynamics adjust in a manner that depends on the adequacy of tissue-level compensation mechanisms. (A) Cerebral blood volume (CBV) can be maintained in mild stages of disease through microvascular autoregulation, which in turn (B) reduces cerebrovascular reactivity (CVR), or the further abilities of vessels to respond to a vasoactive stimulus. (C) When CVR is exhausted, cerebral blood flow (CBF) reduces if CPP reduces further. (D) Throughout these stages, microvascular atherosclerotic burden and/or damage to arteriolar smooth muscle may lead to increases in CVR<sub>DELAY</sub>, or the time required for microvessels to vasodilate. (E) When these mechanisms become collectively inadequate to maintain sufficient oxygen delivery to tissue, the oxygen extraction fraction (OEF; ratio of oxygen consumed to oxygen delivered) will begin to increase.

**Table 1**

Summary of relevant physiological values for many cerebrovascular reactivity imaging protocols. Cerebral hemo-metabolic (Derdeyn et al., 2002; Donahue et al., 2017a; Leenders et al., 1990) and gas exchange values (Guyton, 1977) are based on approximate literature ranges.

| Parameter                                                                                                 | Units                                                        | Typical range                                         |
|-----------------------------------------------------------------------------------------------------------|--------------------------------------------------------------|-------------------------------------------------------|
| <i>Hemodynamic and metabolic parameters</i>                                                               |                                                              |                                                       |
| Cerebral blood flow                                                                                       | ml blood/100 g tissue/min                                    | 35–60 (gray matter)<br>17–28 (white matter)           |
| Cerebral blood volume                                                                                     | ml blood/100 g tissue                                        | 3.5–6.6 (gray matter)<br>2.1–3.0 (white matter)       |
| Cerebral metabolic rate of oxygen                                                                         | ml O <sub>2</sub> /100 g tissue/min                          | 2.8–5.0 (gray matter)<br>1.2–1.7 (white matter)       |
| Oxygen extraction fraction                                                                                | (O <sub>2</sub> consumed/O <sub>2</sub> delivered; unitless) | 0.35–0.44 (gray matter)<br>0.31–0.42 (white matter)   |
| <i>Parameters relevant to gas tension experiments</i>                                                     |                                                              |                                                       |
| Partial pressure of carbon dioxide in arterial blood (PaCO <sub>2</sub> )                                 | mmHg                                                         | 35–45                                                 |
| Partial pressure of oxygen in arterial blood (PaO <sub>2</sub> )                                          | mmHg                                                         | 75–100                                                |
| Partial pressure of carbon dioxide in venous blood (PvCO <sub>2</sub> )                                   | mmHg                                                         | 40–50                                                 |
| Partial pressure of oxygen in venous blood (PvO <sub>2</sub> )                                            | mmHg                                                         | 30–40                                                 |
| End-tidal CO <sub>2</sub> (EtCO <sub>2</sub> )                                                            | mmHg                                                         | 35–45                                                 |
| Blood pH                                                                                                  | -log[H <sup>+</sup> ] (unitless)                             | 7.34–7.44                                             |
| Tissue pH                                                                                                 | -log[H <sup>+</sup> ] (unitless)                             | 7.0–7.1                                               |
| <i>Partial pressures of respiratory gases as they enter and leave the lungs (total pressure 760 mmHg)</i> |                                                              |                                                       |
| Atmospheric air: N <sub>2</sub> /O <sub>2</sub> /CO <sub>2</sub> /H <sub>2</sub> O                        | mmHg                                                         | 597.0/159.0/0.3/3.7                                   |
| Humidified air: N <sub>2</sub> /O <sub>2</sub> /CO <sub>2</sub> /H <sub>2</sub> O                         | mmHg                                                         | 563.4/149.3/0.3/47.0                                  |
| Alveolar air: N <sub>2</sub> /O <sub>2</sub> /CO <sub>2</sub> /H <sub>2</sub> O                           | mmHg                                                         | 569.0/104.0/40.0/47.0                                 |
| Expired air: N <sub>2</sub> /O <sub>2</sub> /CO <sub>2</sub> /H <sub>2</sub> O                            | mmHg                                                         | 566.0/120.0/27.0/47.0                                 |
| <i>Other parameters relevant to reactivity experiments</i>                                                |                                                              |                                                       |
| Pressure at sea level                                                                                     | mmHg                                                         | 760                                                   |
| Room air composition                                                                                      | Percent by volume                                            | 78.1 (Nitrogen)/20.9 (Oxygen). CO <sub>2</sub> = 0.03 |
| Hematocrit                                                                                                | Percent                                                      | 40 - 52% (male); 37–46% (female)                      |
| Hemoglobin                                                                                                | g/dL                                                         | 13.2–6.2 (male)<br>12.0–15.2 g/dL (female)            |

2003; Lu and Ge, 2008; Merola et al., 2016), however approaches remain underdeveloped for clinical applications or have poor spatial specificity. As such, alternative methods remain popular. CVR measurements can describe how near parenchyma is to exhausting reserve capacity, or being able to increase CBF further in response to ensuring reductions in oxygen delivery.

### Approaches for eliciting cerebrovascular responses

To evaluate CVR, external agents are most commonly utilized to induce changes in microvascular resistance using two major classes of stimuli: intravenous pharmacological agents or respiratory challenges. In this section, we discuss stimuli from both classes, their mechanisms of action, and the advantages and disadvantages of each.

**Acetazolamide.** Acetazolamide (ACZ), a reversible carbonic anhydrase inhibitor which catalyzes the conversion of CO<sub>2</sub> into bicarbonate (Itada and Forster, 1977), is the most common pharmacological agent for eliciting vasodilation (Swenson, 2014). Following intravenous ACZ injection, carbonic acid increases and pH decreases, leading to reduced vascular resistance and vasodilation in compliant microvasculature (Settakis et al., 2003). The decrease in pH may occur due to the increased presence of carbonic acid that occurs as a result of carbonic anhydrase inhibition in red blood cells or directly in the vessel walls. A decrease in pH is thought to obstruct the voltage-gated calcium channels in vascular smooth muscle (Klockner and Isenberg, 1994), stopping the influx of calcium ions needed to constrict smooth muscle (Koller and Toth, 2012) and causing relaxation of the smooth muscle and vasodilation (Klockner and Isenberg, 1994). ACZ is most frequently administered as an intravenous injection, with a dosage of approximately 1000 mg being sufficient for maximal dilative effect (Settakis et al., 2003), and imaging is performed 15–20 min after administration (Federau et al., 2017; Settakis et al., 2003). Higher doses of up to 2000 mg have been utilized (Boles Ponto et al., 2004) and frequently doses are applied based on patient size at a ratio of approximately 16 mg/kg. The advantages of ACZ are that it is generally well-tolerated by patients with minimal side effects, respiratory discomforts, and most importantly it is easy to administer as no cooperation is required from the subject (Settakis et al., 2003). Disadvantages of ACZ are that it is contraindicated in a subgroup of patients with kidney disorders, hypercholeremic acidosis, hypokalemia, and hyponatremia; must be considered in the context of drug interactions, specifically amphetamines and other carbonic anhydrase inhibitors; and cannot be easily reversed if patient discomfort is a problem. Eliciting vasodilation with ACZ remains the most common protocol in the clinic, however ACZ is becoming less utilized in research settings owing to emerging respiratory stimuli that can be administered more quickly and with greater flexibility.

**Breath hold.** The most basic method for modulating pCO<sub>2</sub> with a respiratory challenge is with a breath hold, and a recent review has summarized breath hold protocols in detail (Urback et al., 2017). Here subjects are generally instructed to exhale followed by breath holding for 10–30s, during which time blood pCO<sub>2</sub> increases. Breath holding has been applied successfully to evaluate volume flow rate changes in healthy adults and its reproducibility evaluated (de Boorder et al., 2004), to understand mechanisms of neurovascular coupling using multi-modal MRI in healthy adults (Donahue et al., 2009), and it has been suggested that recurrent ischemic events in patients with carotid occlusion may be predicted by changes in MCA flow velocities during breath holding (Vernieri et al., 1999). The advantages of breath holds are that they are easy to administer and do not require exogenous contrast agents or respiratory equipment, and advanced analysis procedures are becoming available for modeling the hemodynamic response function in response to breath hold or more complex breathing tasks (Bright et al., 2009; Pinto et al., 2016). Disadvantages of breath holds are that they must be short given limited abilities of subjects to hold their breath and in turn allow for few measurements or require without multiple repeats, are sensitive to subject compliance, will induce a gradient rather than constant pCO<sub>2</sub>

increase over the challenge duration, and are themselves a motor task and thus are mediated by neuronal and vascular responses in motor cortex and associated regions of the motor network. Generally breath hold stimuli are used for convenience when ACZ or more controlled respiratory challenges may not be feasible due to logistical reasons; they are generally not the stimulus of choice for controlled CVR studies when other avenues are feasible.

**Hypercapnic normoxia.** Inhalation of hypercapnic normoxic gas (e.g., 4–7% CO<sub>2</sub> with balance room air) can be used to quickly increase pCO<sub>2</sub> in arterial blood (within several seconds), eliciting vasodilation in healthy vasculature. These gas mixtures will generally increase end-tidal CO<sub>2</sub> (EtCO<sub>2</sub>) by 5–15 mmHg, however the precise changes will depend on how effectively the gas is administered and individual physiology. Such stimuli will elicit a moderate CBF increase in healthy tissue of 10–50% on average, however the change may vary widely and depend on vascular compliance and reserve capacity. These changes, unlike breath holds which may have a neuronal component in motor regions, elicit a negligible-to-small change in CMRO<sub>2</sub> globally (Kety and Schmidt, 1948; Peng et al., 2017).

**Normocapnic hyperoxia.** Inhalation of hyperoxic gas (e.g., >21% O<sub>2</sub> but typically 50–100% O<sub>2</sub>) with a balance of nitrogen will have a negligible change on arterial oxygen saturation fractions in healthy blood as arterial oxygen is already nearly fully saturated, however will increase oxygen saturation fractions in hypoxic subjects or when Y<sub>a</sub> < 98–100%. Similar to hypercapnic normoxia, the normocapnic hyperoxic effect is believed to be largely isometabolic. The small vasoconstrictive effect of oxygen over short periods is frequently considered negligible. Normocapnic hyperoxic stimuli may cause small reductions in CBF if maintained owing to the effect of oxygen increasing vascular resistance (Kety and Schmidt, 1948), however MRI studies have shown that these changes are small and generally less than 10% even for extreme hyperoxic gas stimuli of 100% (Bulte et al., 2007b). The advantages of hyperoxic stimuli are that they are relatively isometabolic with a small change on vascular tone when applied over short durations, can be tolerated well by patients, and can be used in MRI experiments to modulate blood oxygenation level and estimate CBV (Bulte et al., 2007a). Disadvantages of hyperoxia include known abilities of this stimulus to reduce blood water T<sub>1</sub>, which can complicate MRI signal interpretation especially for ASL (Siero et al., 2015b). At a more fundamental physiological level, hyperoxia can lead to shifting of Hb dissociation curves and oxygen toxicity, and as such hyperoxic stimuli in CVR experiments are generally restricted to no more than a few minutes where such toxicity effects are relatively benign.

**Hypercapnic hyperoxia.** A hypercapnic (e.g., CO<sub>2</sub> fraction 4–7%) hyperoxic (e.g., O<sub>2</sub> fraction > 21% and typically 50–95%) stimulus, with balance nitrogen, is also possible and is most common in cancer applications. The most popular variant of this stimulus is carbogen-5, which consists of 5% CO<sub>2</sub> and 95% O<sub>2</sub>. Such stimuli have been shown to increase oxygen delivery to tissue due to the vasodilatory effects of hypercapnia and elevated blood oxygen provided by the hyperoxic component, however these benefits are likely small for typical scans over short stimulus durations (Ashkanian et al., 2008). Administration of a hypercapnic hyperoxic gas mixture for BOLD-weighted assessment of CVR introduces several experimental confounds because of the hyperoxic component including (i) higher venous HbO<sub>2</sub> and elevated partial pressure of venous oxygen (PvO<sub>2</sub>) from increased O<sub>2</sub> dissolved in plasma, (ii) changes in vascular and tissue susceptibility, and (iii) decreased blood water T<sub>1</sub> due to increased O<sub>2</sub> dissolved in plasma in MRI experiments (Faraco et al., 2015). Advantages of hypercapnic hyperoxia are that this gas mixture can be found readily at most medical centers in the form of carbogen-5, which is a common human prescription drug, which is not the case for other hypercapnic normoxic gas stimuli that may require additional testing and approval for human use. Disadvantages of hypercapnic hyperoxia pertain to the more complex effects that the interaction of elevated pCO<sub>2</sub> and pO<sub>2</sub> may have, including considerations regarding the Haldane effect, changes in oxygen saturation and blood T<sub>1</sub> in a manner unrelated to vascular compliance, and these CVR protocols still

require research approval and consent at most hospitals, as CVR mapping is considered off-label use of carbogen-5.

In terms of safety, pharmacological induction of vascular changes using ACZ are commonly performed in most major clinical centers, frequently during SPECT perfusion imaging (Bonte et al., 1988; Chollet et al., 1989; Suga et al., 2007). ACZ has a biological half-life of 2–4 h and is clinically implicated in many patients for treatment of glaucoma, heart failure, epilepsy, and high altitude sickness. Contraindications are liver or kidney disease, adrenal insufficiency, hyponatremia, hypokalemia, and hyperchloremic acidosis. Drug interactions must also be considered. While sulfonamide allergy has been considered a contraindication for ACZ administration (Settakis et al., 2003), recent literature (Platt and Griggs, 2012) has shown that ACZ may be safely utilized in patients with a history of allergy to sulfonamide.

CVR measurements using hypercapnia have generally reported minimal or no serious complications, with most complaints related to claustrophobia and general discomfort with the facemask apparatus rather than induction of any major neurological or cardiovascular events. In a study of 294 patients (age range = 9–88 years) with cerebrovascular disease; primarily comprised of patients with atherosclerosis, moyamoya, arteriovenous malformation, vasculitis, aneurysm or dissection; scanned using a hypercapnic normoxic stimulus delivered with a computer-controlled rebreathing apparatus, transient symptoms consisting of shortness of breath, headache, or dizziness were observed in 11.1% of subjects during the hypercapnic stimulus, and no evidence of other neurological or cardiovascular symptoms during or immediately after the task were observed (Spano et al., 2013). In a separate study of 92 patients with symptomatic intracranial stenosis scanned using a hypercapnic hyperoxic stimulus delivered from compressed cylinders and clinical-grade oxygen facemasks, no immediate stroke-related complications were reported in response to the respiratory stimulus and longer-term neurological events fell within the range for expected events in this patient population (Donahue et al., 2014a). Major contraindications for hypercapnic respiratory stimuli are chronic obstructive pulmonary disease, inflammatory airway diseases such as asthma, high blood pressure at the time of the exam (generally > 200 mmHg systolic) due to the known effect of hypercapnia to increase blood pressure slightly, and low arterial blood oxygen saturation fractions (< 88%). Breath hold considerations are similar as for these hypercapnic stimuli as well.

The emerging data on safety of CVR experiments suggests that these scans pose low risk to chronic ischemic patients, however larger scale studies that involve multiple centers, and also with surveillance, will be necessary to define the absolute risk and outline more rigid inclusion and exclusion criteria. Additionally, safety considerations in acute or hyperacute stroke patients have not been performed, and there is no evidence that these challenges are implicated or safe in patients experiencing acute stroke symptoms.

While intravenous agents are straightforward to administer, procedures for administering respiratory stimuli have not been standardized across centers. Breath hold stimuli are generally cued either over the scanner intercom or visually using a projector system and mirror, and in most cases last 10–30 s depending on subject compliance, and initiate following an exhale, which will cause pCO<sub>2</sub> to increase faster.

Gas challenges are more variable, and a controlled comparison study of the most common methods has not been undertaken, especially in patients with cerebrovascular disease. The simplest approach is to obtain pre-mixed hypercapnic normoxic (e.g., 5% CO<sub>2</sub>/21% O<sub>2</sub>/74% N<sub>2</sub>) or hypercapnic hyperoxic (e.g., 5% CO<sub>2</sub>/95% O<sub>2</sub>) gases from gas suppliers certified to deliver medical grade mixtures of these gases. It should be noted that *clinical grade* gases are designed for calibration of clinical equipment but not for human consumption, and therefore *medical grade* mixtures should be requested and not all suppliers have certification to produce hypercapnic normoxic mixtures. Gases can be delivered from compressed cylinders located outside the scan room through tubing that enters the scan room or from a Douglas bag inside the scan room. Gases

can be delivered through clinical grade tubing to a clinical grade oxygen face mask, typically at a flow rate of 10–15 L/min. It is necessary to simultaneously measure the EtCO<sub>2</sub> and in some cases fraction inspired O<sub>2</sub> (FiO<sub>2</sub>) using a nasal cannula and standard clinical or research monitoring equipment; setups for such experiments have been used in the literature, and have been shown to be largely reproducible (Donahue et al., 2014b; Tancredi et al., 2014), easy to implement in clinical settings, and to elicit EtCO<sub>2</sub> changes of approximately 5–7 mmHg (Faraco et al., 2015) for CO<sub>2</sub> gas fractions of 5%, however these changes are dependent on the mask and setup, and inter-subject variation is typically on the order of 1–2 mmHg standard deviations. A relatively simple yet reproducible design has been implemented by Tancredi et al. (Tancredi et al., 2014; Tancredi et al., 2015), and this setup comprises a relatively straightforward system that can be implemented using clinical-grade equipment and applied in both research and clinical settings at low cost. In addition, the gas can be delivered to the subject using a diving mouth piece and nose clip (Yezhuvath et al., 2009). Here the source of the gas is similar, but the subject receives the gas through the mouth with the nose closed. This can in many cases provide a more controlled system, albeit at the cost of some additional subject discomfort. The major advantages to delivering pre-mixed gas compositions through standard facemasks or mouthpieces is that the setup is relatively straightforward and pre-scan calibrations or preparations are minimal, and as such these studies can be performed as part of standard clinical protocols with only a moderate increase in scan time or complexity. The disadvantages primarily pertain to mild discomfort, ensuring that the volunteer can fit in the coil comfortably with the mask or mouthpiece, and some variation in EtCO<sub>2</sub> changes that are elicited primarily due to differences with how tightly adhered the delivery device is and subject compliance. When setups are carefully applied and EtCO<sub>2</sub> is monitored and corrected for in post-processing, these setups can provide data that are sensitive to CVR in patients with cerebrovascular disease.

More complex gas delivery systems are also possible. Wise et al. (2007) have elegantly outlined an end-tidal forcing system, in which gas mixtures are titrated to the subject based on individual physiology and the measured EtCO<sub>2</sub> changes. The advantage of this system is that the gas delivery can be assured to be the same in every subject as long as the monitoring equipment is accurate. The disadvantage is that the setup can be cumbersome and is generally not possible to implement for routine clinical scanning. However, when very controlled experiments of cerebral physiology are of interest in a research setting, this setup offers more flexibility and control than the above pre-mixed gas approaches. Finally, computer controlled rebreathing devices have been developed and exploit similar principles of the subject's specific physiology and respiration to target changes in blood gases to a higher level of accuracy (approximately reported as 1 mmHg accuracy in CO<sub>2</sub> targeting for most subjects). Reviews of these devices are available and should be referred to for the interested reader (Fierstra et al., 2013). The disadvantages of these systems are that they require more setup than the standard compressed cylinders and facemask options, require equipment that is currently not FDA-approved, and are more expensive than the above setups. The advantages are that they can provide a more controlled stimulus, which could be especially important when comparing results between centers or interrogating subtle differences in CVR.

#### Neuroimaging approaches for recording cerebrovascular responses

Once a stimulus is chosen, there are several approaches available for measuring the resulting physiological response.

*Positron emission tomography (PET).* PET is a molecular imaging modality that utilizes a biological compound, typically introduced through intravenous injection or inhalation, that has been tagged with a radioactive isotope to image the distribution of that compound in the body. PET radioactive isotopes undergo positron decay, and the emitted positrons travel a short distance in the body before encountering and

annihilating with an electron in the surrounding tissue, an interaction that releases two gamma photons of specific energy in anti-parallel directions. These photon-pairs are detected at approximately the same time. Of particular interest to CVR imaging,  $^{15}\text{O}$  is a radioactive isotope of oxygen and  $^{15}\text{O}$ -water PET can be used to assess CBF (Ter-Pogossian and Herscovitch, 1985). To measure CVR, CBF images are acquired with  $^{15}\text{O}$ -water at baseline and following administration of the vasoactive stimulus, and CVR is calculated as the relative difference between CBF at baseline and CBF during the stimulus (Boles Ponto et al., 2004). The advantage of  $^{15}\text{O}$ -water PET is that CBF can be measured directly and quantitatively (Boles Ponto et al., 2004), and PET is generally considered the gold-standard of CBF imaging in humans. The major disadvantage of  $^{15}\text{O}$ -water PET is the short half-life of  $^{15}\text{O}$  (approximately 2 min), which limits studies with  $^{15}\text{O}$ -water to specialized centers where on-site cyclotrons are capable of producing this tracer (Hsu, 2013). Additional disadvantages pertain to the requirement for an arterial line for accurate quantification, requirement for ionizing radiation and exogenous contrast, need for an additional MR or CT scan for anatomical localization, and limited spatial resolution after post-processing. For these reasons PET CBF and CVR mapping are not performed as frequently as other approaches.

**Single photon emission computed tomography (SPECT).** SPECT is a molecular imaging modality that utilizes a biological compound introduced through intravenous injection, inhalation or ingestion. Unlike PET, the radioactive isotopes utilized in SPECT undergo decay via isomeric transition in which the radioactive isotope decays from a metastable state with higher energy to a more stable state through the emission of a gamma photon. These photons are detected using a rotating Anger camera, and the data are reconstructed to form an image of the compound distribution. The most common SPECT compounds utilized for CVR imaging are  $^{99\text{m}}\text{Tc}$ -exametazime,  $^{99\text{m}}\text{Tc}$ -bicisate, and  $^{123}\text{I}$ -iodoamphetamine (Boles Ponto et al., 2004). SPECT data using one of these compounds are acquired at baseline and after administration of a vasoactive stimulus, and, similarly to PET, CVR is computed as the percent difference between CBF during stimulus and baseline (Hashimoto et al., 2017). The advantages of SPECT are that these radioactive isotopes have much longer half-lives than those utilized in PET. ACZ SPECT is also the most common method for assessing CVR in the clinic and SPECT contraindications are extremely limited. Disadvantages of SPECT for measuring CVR is that it may be performed over two days due to the kinetics of the radioisotopes utilized, requires ionizing radiation, and contrast agents introduced may cause a moderate rise in blood pressure in some patients (Ma et al., 2007).

**Transcranial Doppler ultrasound (TCD).** TCD is a noninvasive technique that utilizes ultrasonic waves and the Doppler effect to measure flow velocity (cm/s). Velocity has been shown to be associated with both CBF and CBV and is computed by measuring the Doppler shift observed in the vessel of interest, such as the MCA (Patrick et al., 1996; Pindzola et al., 2001). CVR is measured with TCD as the percent change in blood flow velocity after administration of a vasoactive stimulus compared to baseline flow velocity, and CVR measurements made with TCD have been utilized as a marker of stroke risk in patients with asymptomatic carotid artery stenosis (Silvestrini et al., 2000). The advantages of TCD are that measurements can be made quickly and with less-expensive equipment. The disadvantages are that it provides a surrogate marker of CBF and that the measurements are highly operator dependent (Pindzola et al., 2001). It is important to note that though often referred to as CBF or CBF velocity, the fundamental measure is that of velocity, rather than CBF as defined earlier as the rate of blood delivery to tissue.

**Arterial spin labeling (ASL) MRI.** ASL MRI is a noninvasive tracer-based technique for quantitative CBF mapping. In ASL, arterial blood water is used as an endogenous, diffusible tracer and is most frequently labeled using either a single radiofrequency pulse (pulsed ASL; PASL) or a train of short radiofrequency pulses (pseudocontinuous ASL; pCASL) (Alsop et al., 2015). The effect of these pulses is to alter the longitudinal magnetization of the inflowing blood water, which then acts as an

endogenous tracer when compared to experiments in which the magnetization is unaltered. Following labeling, a post-labeling delay (PLD) of 1.5–2.5 s is allowed in which the labeled blood water protons are delivered to capillaries and exchange with tissue water. A short echo time, fast readout is then used to acquire flow-weighted images. These labeled images are then compared with control images in which inflowing blood water is not labeled, with the difference providing CBF-weighted maps which can then be converted to absolute units of ml/100 g/min upon application of the flow-modified Bloch equation (Alsop et al., 2015). Therefore, dynamic ASL scans where CBF images are acquired on and off vasoactive stimulus can be used to measure CBF for baseline and hyperemic conditions. The advantages of ASL are that it is noninvasive and provides a direct, quantitative measure of CVR by measuring changes in CBF before and during the vasoactive stimulus with an effective temporal resolution of 4–8 s in most scans. The major disadvantage of ASL is that it is limited by the lifetime of the endogenous tracer, which is determined by the longitudinal relaxation time of arterial blood water (~1.2 s at 1.5 T, ~1.6 s at 3.0 T, and ~2.3 s at 7.0 T) (Lu et al., 2004; Rane and Gore, 2013). This is detrimental in patients with steno-occlusive arterial disease where blood arrival times are much longer than the tracer lifetimes, resulting in a major loss in signal-to-noise ratio (SNR) in the ASL images and rendering the CBF value unreliable unless sufficiently long PLDs are used (Fan et al., 2017).

**Blood oxygenation level-dependent (BOLD) MRI.** BOLD MRI is the most popular method for functional neuroimaging in humans. However unlike ASL, BOLD provides a non-quantitative marker of CVR. BOLD exploits the physiological phenomena that increases in CBF exceed increases in CMRO<sub>2</sub> for strong neuronal or vascular stimulation. Therefore, a larger fraction of oxyhemoglobin (HbO<sub>2</sub>), relative to deoxy-hemoglobin (dHb), is present in capillaries and veins. As HbO<sub>2</sub> is diamagnetic and dHb is paramagnetic, this leads to an increase in blood water T<sub>2</sub> and T<sub>2\*</sub> in capillaries and veins, and thus an increase in the surrounding water signal. As arterial blood is nearly fully oxygenated, changes in blood oxygenation occur primarily in capillaries and draining veins as a result of the well-known mismatch in CMRO<sub>2</sub> and CBF for both neuronal and vascular stimuli. Therefore, the BOLD signal is spatially localized to draining veins, and thus provides only a surrogate marker of CBF and CVR, which co-localize physiologically with the capillary and smooth muscle-lined arteriolar compartments. The BOLD effect is also complex as it reflects a balance of changes in multiple physiological parameters, including CBF, CBV, and CMRO<sub>2</sub>, and therefore contrast must be interpreted in the context of this hemodynamic window with the understanding that different combinations of parameter changes may yield similar ensemble BOLD responses (Blicher et al., 2012). The BOLD response also varies with field strength, with nearly 100% of the BOLD effect being extravascular at ultra-high human field strengths of 7.0 T at typical TE greater than 20 ms, but approximately 70% extravascular at 3.0 T, and 50% extravascular at 1.5 T. The reason for this phenomenon is that the T<sub>2\*</sub> of blood decreases rapidly with increasing magnetic field strength, but the tissue T<sub>2\*</sub> decreases more slowly. At high field strength there is a larger fraction of signal originating from the extravascular compartment. Therefore, the BOLD effect is not directly comparable between field strengths. The advantages of BOLD are that it is noninvasive, simple to perform, and provides a robust signal, and an example of BOLD CVR mapping in cerebrovascular disease is shown in Fig. 4.

**Phase-contrast MR angiography.** Phase-contrast MR angiography is a noninvasive technique that utilizes bipolar gradients to manipulate the phase of flowing spins in a velocity-dependent manner and is useful for measuring flow velocities in large vessels. These flow velocities can then be used to calculate volumetric blood flow to the brain when measured in the ICAs and basilar artery, and CBF can be determined by normalizing this volume flow by the volume of brain tissue. Baseline phase-contrast MR data have been employed for assessment of hemodynamic impairment in patients with steno-occlusive disease (Guppy et al., 2002) but can also provide a reliable measure of CVR (Spilt et al., 2002) when used dynamically in conjunction with a vasoactive stimulus. Studies utilizing

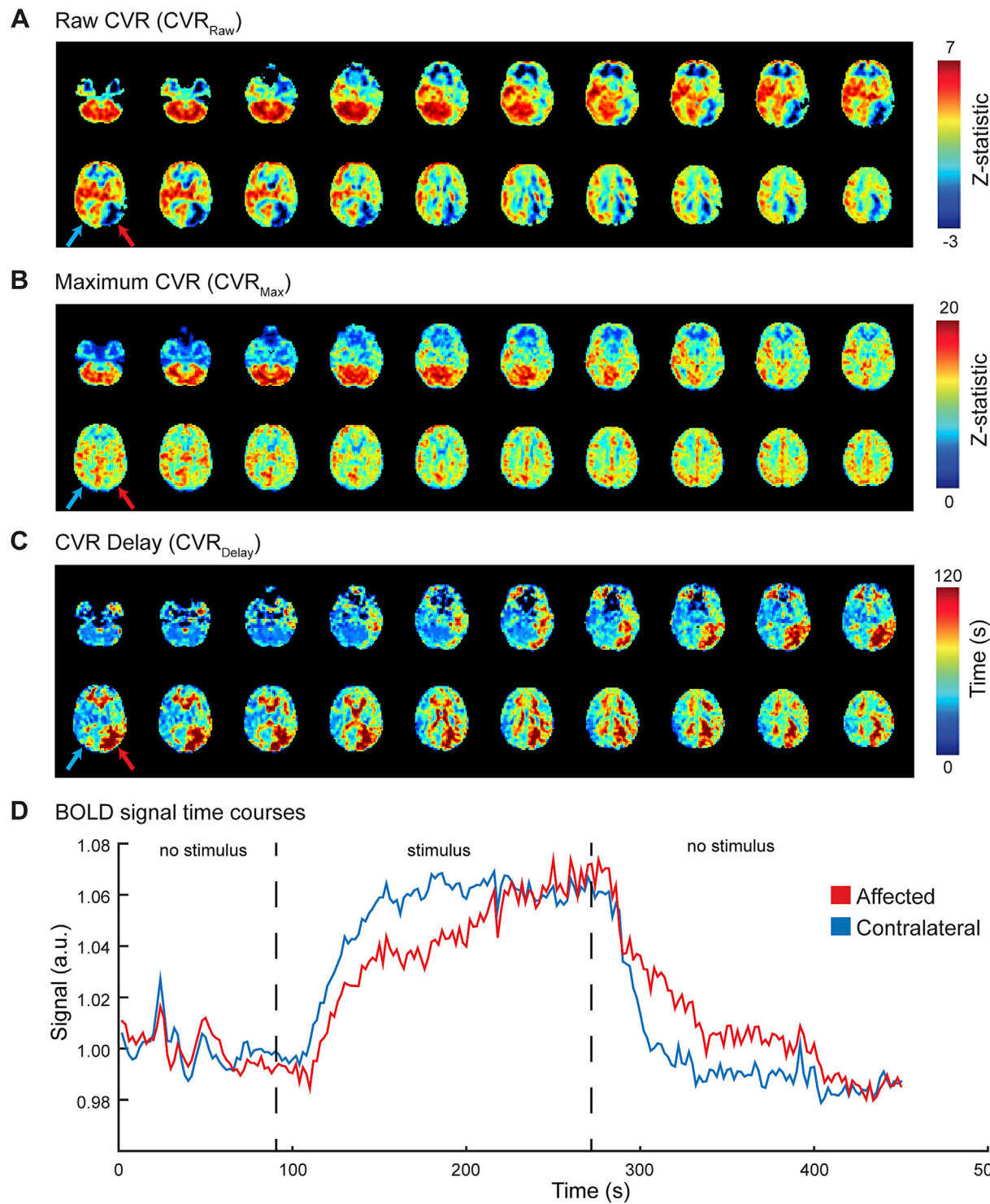


**Fig. 4.** Blood oxygenation level-dependent (BOLD) MR images acquired for cerebrovascular reactivity (CVR) imaging may be analyzed using either a conventional approach where the stimulus paradigm or  $\text{EtCO}_2$  change is applied as the regressor, or in a time-regression approach where the regressor is progressed in time, and maximum correlation and time to maximum correlation (delay) are separately quantified. Representative cases of (A) raw CVR using a pre-defined regressor from the stimulus timing ( $\text{CVR}_{\text{Raw}}$ ), (B) maximum CVR ( $\text{CVR}_{\text{Max}}$ ) from when the time-progressed regressor maximally corresponds with the timecourse, and (C) time-to-maximum CVR ( $\text{CVR}_{\text{Delay}}$ ) maps are shown here for a 52-year old Caucasian male with primary moyamoya disease acquired with hypercapnic stimulus.  $\text{CVR}_{\text{Raw}}$  images show reduced CVR-weighted signal in the left anterior and posterior flow territories compared to the contralateral flow territories. While the  $\text{CVR}_{\text{Max}}$  is marginally reduced in the affected region, a greater difference is observed in the  $\text{CVR}_{\text{Delay}}$  of the affected region compared to the non-affected region. BOLD signal time courses, normalized to baseline, are shown for the affected region and contralateral region across two baseline blocks and one stimulus block. In the affected region, the signal ultimately reaches a similar level compared to the contralateral region but takes longer to achieve this maximum response, potentially indicating delayed blood arrival times and impaired smooth muscle or endothelial response to vasoactive stimuli.

breath holding (de Boorder et al., 2004) and ACZ (Marstrand et al., 2001; Spilt et al., 2002) have demonstrated that increases in the total volume flow to the brain can be detected using phase-contrast MR. The advantage of phase-contrast MR, compared to flow velocity-based measures such as TCD, is that it is less operator dependent and provides sensitivity to a broader number of vessels (de Boorder et al., 2004). The disadvantages are that it is more expensive than TCD, limited to large vessels, can be sensitive to the velocity encoding gradient and direction, and also is frequently averaged over the cardiac cycle providing measures of mean flow velocity rather than peak flow velocity unless appropriate corrections are applied (Enzmann and Pelc, 1991).

### Imaging parameters and analysis considerations

CVR mapping using ACZ SPECT is available in most major radiology departments and quantification procedures are relatively standardized. MRI methods in conjunction with ACZ or hypercapnic challenges have gained popularity in research settings however aside from isolated clinical centers are not offered as billable clinical protocols, owing largely to the novelty of these methods and, for respiratory stimuli, a lack of standardization of gas delivery protocols and analysis procedures. For this reason, much work is beginning to focus on standardizing MRI-based measures of CVR.

In the CVR mapping literature, there is a great deal of emphasis on standardizing respiratory stimuli, but comparatively less emphasis on standardizing acquisition methods and post-processing strategies, which are just as, if not more, relevant as the respiratory setup itself. For instance, error in stimulus delivery will always persist especially in clinical scenarios where patient compliance can be variable, however if the physiological parameters of interest (e.g., EtCO<sub>2</sub>, FiO<sub>2</sub>, CBF, CBV, OEF, etc.) are measured accurately, then much of this variation can be accounted for in analysis. Methods that use only one parameter, especially the BOLD signal change, will always have some degree of variability between centers and scans owing to the qualitative nature of this measurement.

The advantage of BOLD MRI is that it is simple to implement, requiring only a long echo time sequence with a temporal resolution (TR) of 2–3s in its most basic form. At 3.0T, a TE = 30–40 ms is generally utilized to maximize contrast-to-noise ratio while limiting susceptibility-induced distortions near sinuses, together with a fast 2D EPI readout. Common parameters that could provide a foundation for consensus in 3.0T BOLD CVR measurements are TE = 30 ms, TR = 1–2s, single-shot gradient echo EPI readout, and spatial resolution = 3 × 3 × 3 mm<sup>3</sup>. Importantly, acquisitions that utilize much lower TEs, presumably chosen to reduce distortions, increase sensitivity to draining veins relative to tissue and microvasculature, and may provide spatial activation maps or patterns not directly comparable to more typical acquisitions with TE chosen to reflect tissue T<sub>2</sub>\* (Rane et al., 2014; Triantafyllou et al., 2005). Newer BOLD implementations with higher temporal and spatial resolution also hold promise, specifically using multiband imaging in which whole-brain temporal resolutions can be reduced to 750 ms or less (Ravi et al., 2016). These implementations have the advantages of sampling higher frequency fluctuations (e.g., cardiac fluctuations) and removing these nuisance fluctuations from analysis (Tong and Frederick, 2014). Additionally, the relatively high temporal resolution of BOLD allows for the timecourse of the hemodynamic response to hypercapnia to be evaluated, and it has been shown that the timecourse of the hypercapnic response may provide information additionally reflective of endothelial and/or smooth muscle function, and this could be altered even for normal vascular reserve capacity (Donahue et al., 2016b).

An additional concern with BOLD CVR mapping is the correct method for generating CVR-weighted maps. As BOLD does not directly measure CBF, BOLD does not measure CVR directly but instead can only provide a CVR-weighted signal and should always be considered in this context. Standard post-processing procedures generally require steps consisting of (i) baseline drift correction using high pass filtering at greater than twice

the frequency of the block stimulus, (ii) motion correction, (iii) slice time correction, and finally (iv) calculation of either the signal change normalized by the baseline signal ( $\Delta S/S_0$ ) or the t-statistic or z-statistic when the time course is compared with a regressor representative of the stimulus paradigm. The regressor may be the measured EtCO<sub>2</sub> response, gas timing itself, or even global hemodynamic response function. Importantly, most gas delivery systems have a lag of 5–15s before the gas is delivered to the subject, and there is an additional lag of 5–15s for the gas to circulate through the blood stream and for a hemodynamic response function in the brain to be generated. Therefore, in all analysis procedures stimulus epochs should be sufficiently long to allow for the signal to plateau, and stimulus blocks of no less than 30s should be used for basic CVR mapping in most cases, but 60–180s may be ideal in cerebrovascular disease patients where vascular compliance and timing can be substantially altered. Alternative methods that evaluate more transient changes in the hemodynamic response function may utilize shorter stimulus paradigms and these are discussed in subsequent sections. The final step in CVR mapping with BOLD is to normalize the measured signal change to allow for comparison between subjects. This can be achieved either by normalizing each voxel by a healthy region or whole-brain response, or more commonly by the EtCO<sub>2</sub> change ( $\Delta \text{EtCO}_2$ ). As such, the final observable from BOLD CVR-weighted mapping is commonly a measure of  $\Delta S/S_0/\Delta \text{EtCO}_2$ .

ASL MRI developments are also occurring with rapid succession and ASL in principle holds greater potential to directly interrogate CVR than BOLD, as it provides an indicator of CBF rather than T<sub>2</sub>(\*)-weighted signal. The most popular CBF implementations utilize pCASL labeling, which exploits a 1–2s string of short radiofrequency pulses with low B<sub>1</sub> to invert inflowing blood water using principles of adiabatic inversion. Post-labeling delays are generally 1.5s–2.0s at 3.0T, however much longer PLDs may be required in the setting of cerebrovascular disease, especially patients with extensive collaterals and delayed blood arrival times. As the endogenous blood water label decays with the T<sub>1</sub> of arterial blood water, increasing the PLD will result in lower SNR at the time of acquisition, and therefore in patients with very delayed arrival times beyond 2–3s, ASL may not be relevant. Another disadvantage of pCASL is the lower temporal resolution relative to BOLD, as pCASL generally has a TR of 4s, and a sequential control and label acquisition must be subtracted to generate a CBF map, which leads to an effective temporal resolution of 8s. Here, subtle changes in vascular compliance timing, as can be interrogated with BOLD, may not be possible. Post-processing procedures with ASL have recently been summarized (Alsop et al., 2015; Donahue et al., 2017b) and include (i) motion correction, (ii) pair-wise subtraction to generate CBF-weighted images, and (iii) conversion of the CBF-weighted images to CBF maps using the solution to the flow-modified Bloch equation. Note that due to the pair-wise subtraction, temporal filtering and baseline drift correction is generally not necessary. Slice-time correction is necessary when 2D readouts are used, but not when single-shot 3D readouts are used with a single excitation pulse per volume and TR (Gunther et al., 2005).

Many of the same readout developments relevant to BOLD (e.g., multiband imaging) can be applied to the ASL readout, thereby increasing temporal resolution. However, the lower temporal resolution of ASL is more inherently limited by the long labeling duration (in pCASL) and PLDs. Vessel-encoded pCASL, in which blood water labeling is achieved separately for different arteries is being pursued for both CBF determination and flow territory mapping (Okell et al., 2013; Wong, 2007), and this approach has also been used in reactivity experiments to determine flow territory stability in response to changes in pCO<sub>2</sub>, as well as CVR of different flow territories (Roach et al., 2015). In this approach, gradients are inserted between pulses in the pCASL labeling module, thereby inducing a phase accrual in the prescribed direction. Spatially-specific labeling efficiency can be achieved by appropriately phase-cycling the RF pulses in the labeling module, and flow territory maps of right and left anterior and posterior territories can be achieved in less than 5 min, and planning-free approaches have been developed and

evaluated for clinical consistency with catheter angiography (Arteaga et al., 2017).

The final observable from ASL CVR studies is commonly the fractional change in CBF normalized by the EtCO<sub>2</sub> change:  $\Delta\text{CBF}/\text{CBF}_0/\Delta\text{EtCO}_2$ . Importantly, as CBF is a physiological parameter, rather than T<sub>2</sub><sup>\*</sup>-weighted signal, it is in principle easier to compare between subjects and time points.

### Applications for cerebrovascular reactivity imaging in cerebrovascular disease

CVR mapping has been applied in multiple applications of cerebrovascular disease. This section is intended to highlight clinical unmet needs in the setting of cerebrovascular disease, and recent work in which CVR mapping is being applied to address these needs.

**Atherosclerotic arterial steno-occlusive disease.** Reducing stroke-related morbidity requires an improved understanding of early biomarkers that predict hemodynamic failure and can be used for prescient identification of patients requiring aggressive, preventative therapy (Goldstein et al., 2009; González, 2005; Lin et al., 2013). For instance, extracranial atherosclerotic disease (ECAD) is a well-known risk factor for stroke; following the North American Stenting vs. Carotid Endarterectomy Trial (NASCET), patients with symptomatic ECAD of the ICA have generally been revascularized surgically, resulting in a 2–4% five-year rate of disabling stroke (1991; Reed et al., 2003; Voeks et al., 2011). However, patients with intracranial (IC) atherosclerotic disease (ICAD) comprise approximately 7–24% of new strokes (Famakin et al., 2009; Kasner and Gorelick, 2004; Liebeskind et al., 2010; Ovbiagele et al., 2008) and unlike patients with ECAD, appropriate ICAD treatment is less clear as a result of the recently-halted SAMMPRIS and VISSIT trials (SAMMPRIS, 2011; Zaidat et al., 2015). In these prospective trials, 14–24.1% of ICAD patients treated with stenting and aggressive medical management (AMM), consisting of anti-platelet and statin therapy, experienced a stroke within 30 days, compared to just 5.8–9.4% of patients receiving AMM alone. However, final results from both trials revealed that even in the AMM arms, approximately 12–15% of patients experienced recurrent stroke in one year (Derdeyn et al., 2014). Due to this high rate of recurrent stroke on standard of care therapies, clinical ICAD research is acutely impactful and there is an immediate need to identify sources of hemodynamic impairment in these patients and use this information to personalize therapies.

Imaging modalities such as TCD, MR angiography, and CT angiography can be used to characterize stenosis degree in ICAD, and severe stenosis has been shown to be associated with downstream hemodynamic compromise (Banerjee and Chimowitz, 2017). However, patients with occluded vessels and impaired CVR may be at higher risk for subsequent stroke compared to those with similar levels of occlusions but uncompromised CVR (Ma et al., 2007). A prospective study utilizing TCD with hypercapnic stimuli demonstrated that 32% of participants with impaired CVR suffered a stroke or TIA compared to 8% of participants with intact CVR (Kleiser and Widder, 1992). In addition to characterizing the effect of atherosclerotic stenosis on tissue-level hemodynamics, CVR imaging may be helpful in assessing whether a given patient with ICAD is a good candidate for aggressive, albeit currently controversial, surgical interventions (Attye et al., 2014; Bouvier et al., 2015; Mandell et al., 2011). Utilizing TCD and SPECT with a breath-hold stimulus, it has been shown that superficial temporal artery (STA)-MCA bypass surgery performed in patients with severe steno-occlusive disease and impaired CVR results in a reduction in stroke recurrence (Low et al., 2015). Therefore, while management of ICAD patients remains controversial, CVR imaging may be of particular interest in this population in identifying those with severe disease who may benefit from aggressive interventions and recent work using hypercapnic BOLD MRI has shown that CVR may be prognostic for recurrent ischemic injury in patients with carotid occlusion (Goode et al., 2016). Future work will likely focus on identifying patients with ICAD at risk of failing standard-of-care AMM and triaging such

patients for more aggressive therapies. Achieving this will require consideration of symptomatology, modifiable risk factors, and neuroimaging markers of hemodynamic failure, possibly including CVR mapping.

**Non-atherosclerotic arterial steno-occlusive disease.** Moyamoya disease (MMD) is a non-atherosclerotic cerebrovascular condition characterized by progressive stenosis of the supraclinoid ICAs and proximal branches, and the corresponding development of elaborate networks of collateral blood vessels (Scott and Smith, 2009). Idiopathic MMD is believed to arise independent to other cerebrovascular conditions and places patients at more than a seven-fold risk increase for stroke (Hallemeier et al., 2006). While idiopathic MMD is relatively rare (incidence < 1 case/100,000 children in North America), Moyamoya syndrome (MMS), which may arise secondary to Down syndrome, sickle cell disease, atherosclerosis, and radiotherapy shares many phenotypical characteristics as idiopathic MMD and is not an uncommon comorbidity in these conditions (Kassim and DeBaun, 2013; Phi et al., 2015). Such patients have a wide clinical presentation and prognosis, which is hypothesized to depend sensitively on the location and extent of steno-occlusion, parenchymal response via development of collateral vessels, and associated comorbidities (Achrol et al., 2009; Scott and Smith, 2009). While recent work has greatly increased our understanding of cerebrovascular disease treatments generally, Moyamoya etiology remains unknown, animal disease models do not exist, biomarkers that may place patients at highest risk for stroke have not been conclusively established, and randomized trials evaluating preferential utility of surgical revascularization variants have not been performed.

There is currently no treatment that is known to halt or reverse MMS. Rather, treatment focuses on improving CBF through medical therapy including antiplatelet agents, calcium-channel blockers, and more rarely anticoagulants (Scott, 2000; Scott et al., 2004). More aggressive surgical revascularization using either direct bypass or indirect synangiosis procedures are performed in patients with symptoms unresponsive to medical therapy (Scott, 2000) and are increasingly utilized (Ikezaki, 2000). The most pressing clinical question in these patients is whether aggressive surgical procedures are required, and if so, how parenchymal hemodynamic and metabolic responses alter stroke risk. Addressing these issues likely requires accurate measurements of how parenchyma compensates for steno-occlusion, including knowledge of moderate-to-large vessel lumen and wall morphology and vascular reserve capacity.

Such non-atherosclerotic conditions represent a popular application of CVR studies (Fig. 5), partly due uncertainties with correct management of these patients and abilities of new methods to provide insights regarding extent of impairment and revascularization candidacy. In response to vasoactive stimuli, SPECT imaging originally demonstrated that CBF reactivity was reduced in moyamoya patients (Hoshi et al., 1994; Tatemichi et al., 1988), and more recently using MRI in conjunction with hypercapnic stimuli, CVR magnitude has been consistently shown to be reduced, and onset of hemodynamic responses delayed, in patients with moyamoya (Cogswell et al., 2017; Donahue et al., 2015; Liu et al., 2017b). CVR timing values have been shown to correlate with arterial circulation times measured from catheter angiography (Donahue et al., 2013) and preliminary scoring systems have been proposed that include CVR as a relevant variable in addition to standard anatomical information from angiography and FLAIR (Ladner et al., 2017). Importantly, delays in maximal hemodynamic responses due to delayed arterial blood circulation times and/or smooth muscle relaxation are frequently observed in moyamoya patients. This effect can manifest as apparent negative responses, sometimes attributable to *vascular steal phenomena*, owing to the hemodynamic signal during the epoch when the stimulus is off being higher than when it is on (owing to extreme delays in onset times). As such, care must be taken in quantifying and interpreting these signal time courses, and time delay analyses may be required (Donahue et al., 2015). ASL MRI has also been shown to provide a sensitive marker of hemodynamic impairment in these patients (Yun et al., 2015),

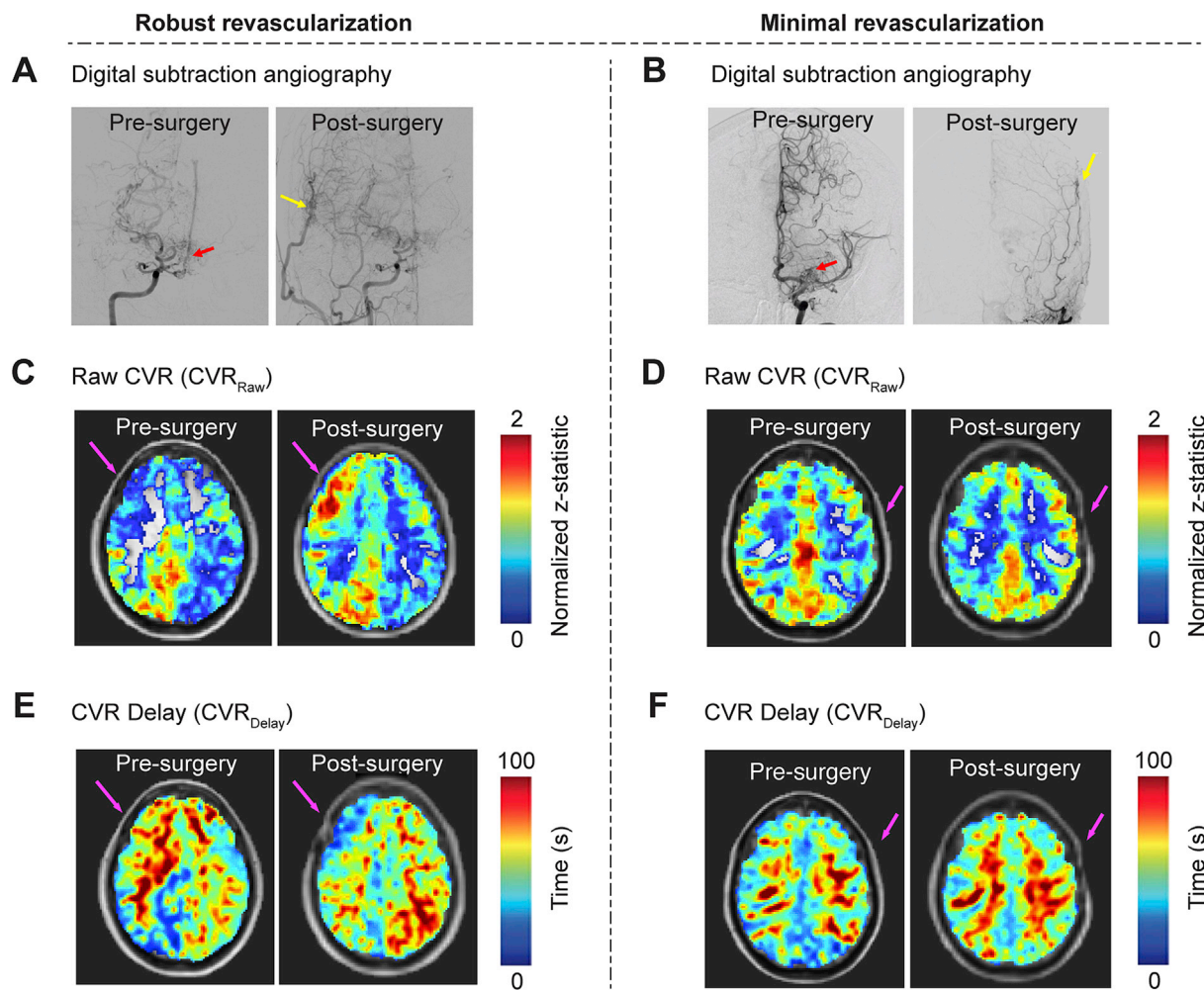


**Fig. 5.** Blood oxygenation level-dependent (BOLD) MRI may be utilized to monitor treatment response in patients with moyamoya disease. (A, B) Representative examples of pre- and post-surgery digital subtraction angiography (DSA), (C, D) raw CVR ( $\text{CVR}_{\text{Raw}}$ ), and (E, F) time-to-maximum CVR ( $\text{CVR}_{\text{Delay}}$ ) maps are shown for two patients: 1) a 28-year old Asian female with primary moyamoya disease and successful right-sided EDAS and 2) a 53-year old Caucasian female with secondary moyamoya disease and unsuccessful left-sided EDAS. Surgical success was determined based on whether 2/3 or more of the MCA territory was perfused following surgery as determined from DSA. For the first patient, success of the revascularization procedure is demonstrated by DSA, and corresponding increases in  $\text{CVR}_{\text{Raw}}$  (C) and decreases in  $\text{CVR}_{\text{Delay}}$  (E) can be seen. For the second patient, the revascularization procedure was unsuccessful based on the post-surgery DSA (B), and this is indicated by the lack of change seen in the  $\text{CVR}_{\text{Raw}}$  (D) and  $\text{CVR}_{\text{Delay}}$  (F) images. This example illustrates the potential of CVR imaging as a marker of treatment response to revascularization surgery in patients with moyamoya disease.

especially when long post-labeling delays are used which account for the delayed blood arrival to tissue (Fan et al., 2017). Data using ACZ and SPECT have shown that improvement in cerebral hemodynamics as assessed by CVR following STA-MCA bypass correspond with improvements in patient symptoms (Kawabori et al., 2013), and hypercapnic stimuli have been applied to show improvements in CVR following direct and indirect revascularization procedures (Donahue et al., 2015; Sam et al., 2015).

**Anemia.** A significant mechanism for stroke in patients with sickle cell anemia (SCA) is hemodynamic imbalance with a reduced supply of oxygen due to reduced oxygen carrying capacity and HbS presence. Known risk factors for stroke specific to SCA include low baseline hemoglobin, acute chest syndrome, anemic crisis, fever, and hypertension (Balkaran et al., 1992; Ohene-Frempong et al., 1998). Adults with SCA also generally have traditional stroke risk factors (Strouse et al., 2009). TCD is frequently used to assess flow velocity in children with SCA, and elevated MCA flow velocities are believed to provide a surrogate marker for initial stroke risk (Adams, 2005). However, TCD provides no direct information on CBF or vascular reserve at the level of the parenchyma, and also TCD does not identify increased risk of infarct recurrence (Adams, 2005; Adams et al., 1998). To address these limitations, more comprehensive tools to evaluate the spectrum of hemo-metabolic changes that occur in

SCA in terms of CVR, CBF, and OEF are likely needed. Cerebral autoregulation maintains CPP so that increases in MAP produce vasoconstriction of pial arterioles, and decreases in MAP produce vasodilation, thus altering resistance and increasing microvascular CBV (Rapela and Green, 1964). In SCA, when arterial oxygen content decreases, CBF and CBV, and thus oxygen delivery, may increase as a result of elevated cardiac output and/or microvascular autoregulation (Vorstrup et al., 1992). OEF will increase if the total oxygen delivery is inadequate and  $\text{CMRO}_2$  is preserved (Derdeyn et al., 2002).

Individuals with SCA and without significant vasculopathy typically have chronically increased CBF (Gevers et al., 2012; Prohovnik et al., 2009; Vorstrup et al., 1992) in a manner that depends on several factors including the balance of oxygen carrying capacity and HbS fraction (Hurlet-Jensen et al., 1994), vasculopathy extent (Arkuszewski et al., 2014), and cerebrovascular reserve (Derdeyn et al., 2002; Gupta et al., 2012). Importantly, these factors influence CBF in opposite ways, with reduced oxygen carrying capacity leading to increases in CBF, while cerebral vasculopathy and reduced autoregulatory capacity can lower CBF. Thus, CBF is not necessarily specific for the source of impairment and identical CBF can have distinct underlying hemodynamic mechanisms. OEF, which reports fundamentally on the ratio of oxygen consumed to that which is delivered, may have added discriminatory

capacity for impairment. Specifically, as CBF becomes insufficient to meet hemodynamic demands, due to any or all of the above causes, there will be a gradient of increasing OEF to maintain a constant CMR<sub>O2</sub> (Derdeyn et al., 2002). Therefore, OEF has been postulated to be a more sensitive indicator of critical tissue-level impairment for cerebral ischemia and eventual strokes compared to CBF or CBV over a larger range of hemodynamic impairment (Derdeyn et al., 2002; Jordan et al., 2016), yet methods for measuring OEF regionally, routinely, and non-invasively have remained elusive.

Given this, CVR methods hold great promise for additionally evaluating how near patients are to exhausting cerebrovascular reserve with the hypothesis that CBV may be near maximal in many patients, and as such CVR in response to vasoactive stimuli will be shunted. Indeed, recent work using BOLD MRI in conjunction with a CO<sub>2</sub> respiratory stimulus has shown that reduced CVR is associated with reduced cortical thickness in 60 children with sickle cell disease compared to 27 age-matched subjects without sickle cell, most prominently in left cuneus, right post central gyrus and the right temporal pole (Kim et al., 2016). Regional associations also revealed that reduced CVR co-localized with brain regions with high metabolic activity, suggesting that such regions could be more prone to hypoxia-induced damage. Work in a cohort of five patients using MRI showed that CBF decreased and CVR increased following blood transfusion, consistent with increases in oxygen carrying capacity of blood being associated with lower demands for autoregulation and in turn increases in reserve capacity (Kosinski et al., 2017). Fig. 6 shows an example of very recent work using ASL MRI before and after ACZ administration in an adult with SCA, demonstrating that such protocols can be used to visualize reduced reserve capacity in the face of elevated CBF (Václavík et al., 2016, 2017).

*Cerebral small vessel disease and aging.* Cerebral small vessel disease (CVSD) is characterized radiologically by the presence of small subcortical lesions, such as white matter hyperintensities and lacunes (Wardlaw et al., 2013b), and vascular endothelial dysfunction has been proposed as a key mechanism for the development of CSVD (Wardlaw et al., 2013a). The fundamental questions in this population are who will develop CSVD and related white matter disease, whether patients with CVSD will

progress, and how this impacts cognitive function and symptomatology. A thorough review of the role for CVR imaging in small vessel disease was recently presented by Blair et al. (Blair et al., 2016). Endothelial dysfunction may result in the stiffening of small blood vessels, causing them to become unreactive to vasoactive stimuli (Blair et al., 2016). Thus, CVR imaging may be ideally suited for studying this possible etiology of CSVD. However, currently-available data are conflicting (Conijn et al., 2012; Hund-Georgiadis et al., 2003) on whether CVR is reduced in patients with CSVD, and Blair et al. (Blair et al., 2016) have identified several key factors affecting comparison of CVR studies in this population, including patient heterogeneity, differences in MR acquisition protocols, the vasodilatory stimulus utilized, and the methods for CVR computation.

Advancing age is the strongest risk factor for cerebrovascular disease and cognitive impairment (Nagata et al., 2016). With the world's population aged 60 years and older rapidly growing, neuroimaging techniques are becoming increasingly utilized for understanding the cerebral hemodynamic changes due to aging. Whole-brain CBF and regional CMR<sub>O2</sub> has been shown to be lower in older adults compared to younger adults (De Vis et al., 2015), and CVR assessed with BOLD MRI and hypercapnic normoxia stimulus has demonstrated age-related decreases in CVR, and this decrease is more prevalent than decreases in CBF (Lu et al., 2011). Studies in cerebral white matter (e.g., Fig. 7) are of particular interest since white matter hyperintensities, which are thought to be associated with CSVD, have been associated with cognitive decline in aging (Sam et al., 2016). Using BOLD MRI and EtCO<sub>2</sub>-controlled delivery of a hypercapnic normoxic stimulus, Sam et al. (Sam et al., 2016) have suggested that baseline CVR is lower in normal-appearing white matter that progressed to pathological white matter hyperintensities at one-year follow-up in a cohort of older adults (age range = 50–91 years); this finding suggests that hemodynamic impairment related may be associated with progression of aging-related white matter disease. Furthermore, Thomas et al. (Thomas et al., 2014) utilized BOLD MRI and hypercapnic stimuli to demonstrate that CVR in the white matter was lower than CVR in the gray matter, with a response delay of ~20s in white matter reactivity compared to gray matter. Interestingly, with

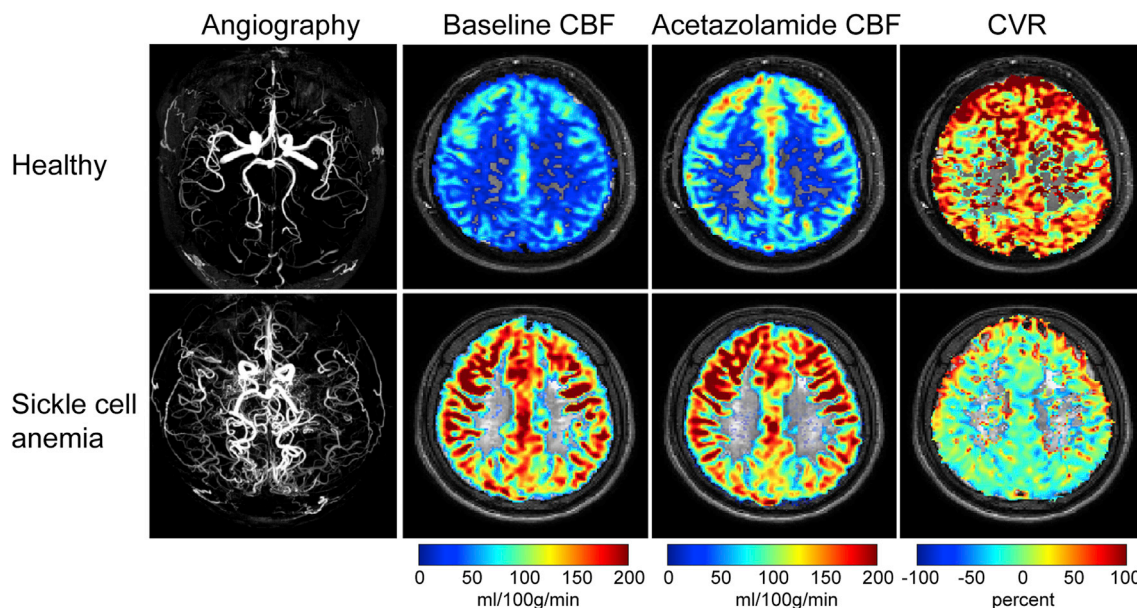


**Fig. 6.** Cerebrovascular reserve in sickle cell disease (SCD). (Above) Intracranial magnetic resonance angiography (MRA) and corresponding cerebral blood flow (CBF) maps at baseline and 10 min following intravenous acetazolamide (dose = 16 mg/kg) infusion in a 24 year old healthy male without a history of cerebrovascular disease or hemoglobinopathy. CVR, defined as the fractional change in CBF in response to acetazolamide, is approximately 80% and largely symmetric throughout gray matter parenchyma. (Below) A 29 year old male with SCD and moyamoya syndrome. MRA shows hypervascularity and baseline CBF is elevated in response to anemia and reduced oxygen carrying capacity. Upon acetazolamide administration, the CBF response is blunted compared to the healthy control, translating to low-to-negligible CVR. These data are consistent with the SCD patient operating at or near cerebrovascular reserve capacity and such patients may be at elevated risk of future ischemic events. Images provided by Lena Václavík and additional information can be found in Václavík L et al. (Václavík et al., 2017).

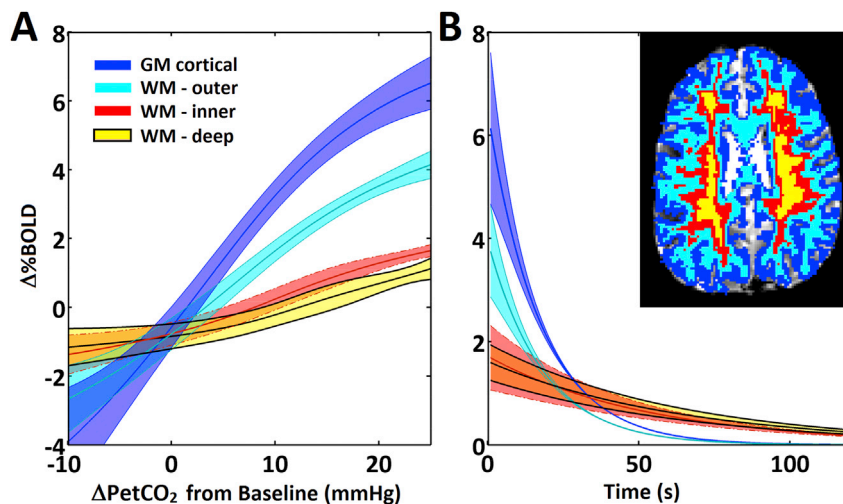


**Fig. 7.** Reactivity in white matter, acquired using 7.0T MRI and adapted from Bhogal et al. (Bhogal et al., 2015). (A) Normalized BOLD-CVR response curves comparing gray matter with white matter of increasing depth averaged across nine subjects. BOLD signal magnitude is reduced at increasing white matter depth. Also, the shape of the response curve shifts to the right at increasing white matter depth. (B) Regions of interest for a single subject are shown in top right inset. Return to baseline decaying exponential curves averaged across nine subjects.

increasing age, CVR response in white matter was faster and increased in magnitude, which was contrary to the finding in gray matter, suggesting that microvascular characteristics may be unique in white matter (Thomas et al., 2014). As white matter CBV and CBF are 2–3 times lower than gray matter CBF and CBV, sensitivity to white matter CVR can be low, requiring higher SNR approaches at higher field strength when evaluated with MRI.

#### New developments and future directions

Developments in the field of CVR are occurring that aim at exploiting not just the magnitude but the temporal dynamics of the hypercapnic response. For instance, it has been shown that while increases in CVR-weighted MRI signal are generally correlated with arterial circulation times from digital subtraction angiography (Donahue et al., 2013), in patients with severe intracranial disease additional delays may be present which could correspond to added time for arterioles to dilate fully in response to vasoactive stimuli. These delays can be on the order of 10s or more, much longer than typical blood arrival times, and may provide a marker of vascular compliance. Recent work has shown that these changes can be just as large or larger than magnitude signal changes, adjust after surgical revascularization, and can be quantified using time regression analysis tools (Donahue et al., 2015). Ongoing work is also focused on using more complex sinusoidal stimulus paradigms to obtain CVR information in shorter scan durations of 3–5 min (Blockley et al., 2017), and these faster methods likely have relevance in healthy and patient studies where reactivity timing is not substantially delayed.

While CVR mapping with respiratory challenges frequently employ a standard hypercapnic stimulus of 5% CO<sub>2</sub>, it is possible that new insights could be gained by using graded hypercapnic challenges where the CO<sub>2</sub> fraction is titrated from baseline (EtCO<sub>2</sub> = 35–45 mmHg) up to elicit a change of as much as 15 mmHg. Such studies may lead to subject discomfort when the stimulus is applied for long durations, but shorter duration graded studies at high spatial resolution and a field strength of 7.0T have been performed successfully and have shown that the BOLD response to progressively increasing changes in PaCO<sub>2</sub> is non-linear (Bhogal et al., 2014). Spatial patterns of differences in linearity with increasing PaCO<sub>2</sub> is also being evaluated at 3.0T (Fisher et al., 2017), and may provide new contrasts relevant to vascular compliance.

Additionally, the burden of performing gas challenges is becoming increasingly realized, despite their utility for interrogating reserve capacity relatively quickly. As such, newer procedures are being investigated which aim to map measures of vascular compliance or regional

blood arrival time differences using baseline images acquired in the absence of any provided stimulus. For instance it has been shown that connectivity analyses can be performed on baseline BOLD images to obtain maps similar to CVR<sub>Delay</sub> maps, but without contrast agents, and these approaches have been demonstrated in patients with MMS (Christen et al., 2013). Resting state networks have also been shown to have relevance for understanding adaptive brain plasticity mechanisms post-stroke, and could provide a marker of functional recovery after stroke which could be useful for triaging patients for plasticity-inducing therapies (Dijkhuizen et al., 2014). Beyond basic timing and functional connectivity analyses, baseline BOLD images have also been used to investigate indicators of CVR itself without the need for stimulus delivery. Here, natural variations in respiration and related baseline BOLD signal characteristics have been shown to correlate significantly with hypercapnia-induced CVR, and thus could provide an indicator of this measure in patients where gas challenges are contraindicated (Golestan et al., 2016; Jahanian et al., 2017; Liu et al., 2017a; Prokopiou et al., 2016). Baseline BOLD measurements have the advantage of being easily implementable, requiring a single-shot gradient echo EPI protocol with intermediate-to-long echo time, and no respiratory or pharmacological stimulus. The current limitation is that more elaborate post-processing is generally required to extract CVR-weighted information, and the final metric is more a measure of vasoactivity and dynamic cerebrovascular activity than cerebrovascular reserve capacity.

The majority of CVR and functional neuroimaging studies generally focus on gray matter responses. However more recent work at intermediate (3.0T) and high (7.0T) human field strengths have begun to investigate white matter signal characteristics (Bhogal et al., 2016). 7.0T MRI is particularly intriguing for this avenue of work, as SNR increases linearly with field strength, and CBF and CBV are generally 2–3 times lower in white matter parenchyma than gray matter parenchyma, and thus smaller white matter hemodynamic changes can be identified in principle with higher fidelity at higher field strength. Additionally, the extravascular source of the BOLD signal at higher magnetic field strength should increase the specificity to capillaries and extravascular tissue, rather than draining veins (Donahue et al., 2011; Duong et al., 2003). The higher SNR afforded at 7.0T should also allow for CVR to be investigated as a function of cortical depth and over much smaller spatial scales, and work in this regard has also been pursued primarily in healthy subjects (Huber et al., 2014, 2015; Siero et al., 2015a). It has been shown that the white matter response is also delayed by several seconds relative to the gray matter CVR response, and white matter CVR may increase with age, whereas gray matter responses decrease with age. White matter CVR

mapping could hold relevance for investigating small vessel disease mechanisms, and specifically sub-clinical changes that may predispose patients for white matter disease later in life (Bhogal et al., 2016; Thomas et al., 2014).

Generally in terms of diagnosis, there is a growing appreciation to understand the complete spectrum of cerebrovascular disease, from prior evidence of ischemic damage and infarction on anatomical imaging, to large vessel steno-occlusion and vessel wall characteristics, and finally to smaller parenchymal hemo-metabolic compensation mechanisms that may be present. A recent consensus statement on this topic and relevant research directions has been published (Donahue et al., 2017a). To achieve this, multi-modal imaging may be relevant, such as using catheter angiography or CT angiography as gold-standard methods for lumenography and PET or MRI for hemo-metabolic and anatomical imaging, respectively. Furthermore, as noninvasive MRI methods continue to be developed, PET hemo-metabolic imaging may be replaced by MRI methods that do not require ionizing radiation and can be performed more easily for routine surveillance, however many methods still require further development and validation.

There is also an interest in improving post-processing procedures to enable online visualization of CVR-related parameters, as well as to be able to interpret findings in the context of normative and abnormal ranges. Most MRI scanner vendors now offer basic graphical fMRI post-processing packages that allow for a general linear model or cross correlation analysis to be applied to dynamic fMRI data, thereby enabling maps to be generated on the scanner and even exported to the hospital PACS with minimal user expertise. ASL MRI maps can also be calculated using online image algebra tools on most scanners, and commercially available software is available for processing of SPECT data. However, more complex analysis tools that perform time regression analysis or extract CVR-weighted information from baseline signals are not available beyond in-house programs generated at specialized centers.

## Conclusions

This document summarizes the physiological changes underlying blood flow regulation in response to reduced oxygen delivery to tissue, and specifically the role of cerebral autoregulation in adapting to such conditions. Abilities to measure surrogates of autoregulation through CVR mapping using PET, SPECT, TCD, and MRI in sequence with pharmacological or respiratory stimuli are possible, and these procedures have been shown to have relevance for interrogating regional hemodynamic impairment and potentially recurrent ischemic damage in patients with arterial steno-occlusive disease, anemia and small vessel disease. In addition, ongoing work is aimed at obtaining CVR metrics without vasoactive stimuli, and such methods hold promise for future neuro-imaging applications. Reducing death and disability associated with cerebrovascular diseases will likely require improved abilities to predict hemodynamic failure in early and therefore treatable stages of disease, and as outlined here CVR mapping holds promise, when combined in sequence with anatomical imaging and angiography, for interrogating multiple-levels of hemodynamic disease and compensation.

## Funding

NIH/NINDS 1R01NS07882801A1, NIH/NINDS 1R01NS097763, NIH/NINR 1R01NR01507901, AHA Southeastern affiliate 14GRNT20150004, AHA National affiliate 14CSA20380466.

## Acknowledgements

We are grateful to Lena Václavů, Jeroen Hendrikse, Jeroen Siero, Alex Bhogal, and Jennifer Watchmaker for providing figures for this document. Funding provided by: NIH/NINDS 1R01NS07882801A1, NIH/NINDS 1R01NS097763, NIH/NINR 1R01NR01507901, AHA Southeastern affiliate 14GRNT20150004, AHA National affiliate

14CSA20380466.

## References

- 1991 Clinical alert: benefit of carotid endarterectomy for patients with high-grade stenosis of the internal carotid artery. National Institute of Neurological Disorders and Stroke Stroke and Trauma Division. North American Symptomatic Carotid Endarterectomy Trial (NASCET) investigators. *Stroke; a journal of cerebral circulation* 22, 816–817.
- Achrol, A.S., Guzman, R., Lee, M., Steinberg, G.K., 2009. Pathophysiology and genetic factors in moyamoya disease. *Neurosurg. Focus* 26, E4.
- Adams, R.J., 2005. TCD in sickle cell disease: an important and useful test. *Pediatr. Radiol.* 35, 229–234.
- Adams, R.J., McKie, V.C., Brambilla, D., Carl, E., Gallagher, D., Nichols, F.T., Roach, S., Abboud, M., Berman, B., Driscoll, C., Files, B., Hsu, L., Hurlet, A., Miller, S., Olivier, N., Pegelow, C., Scher, C., Vichinsky, E., Wang, W., Woods, G., Kutlar, A., Wright, E., Hagner, S., Tighe, F., Waclawiw, M.A., et al., 1998. Stroke prevention trial in sickle cell anemia. *Control Clin. Trials* 19, 110–129.
- Alsop, D.C., Detre, J.A., Golay, X., Gunther, M., Hendrikse, J., Hernandez-Garcia, L., Lu, H., MacIntosh, B.J., Parkes, L.M., Smits, M., van Osch, M.J., Wang, D.J., Wong, E.C., Zaharchuk, G., 2015. Recommended implementation of arterial spin-labeled perfusion MRI for clinical applications: a consensus of the ISMRM perfusion study group and the European consortium for ASL in dementia. *Magn. Reson Med.* 73, 102–116.
- Aoyama, Y., Ueda, K., Setogawa, A., Kawai, Y., 1999. Effects of pH on contraction and Ca<sup>2+</sup> mobilization in vascular smooth muscles of the rabbit basilar artery. *Jpn. J. Physiol.* 49, 55–62.
- Arkuszewski, M., Krejza, J., Chen, R., Ichord, R., Kwiatkowski, J.L., Bilello, M., Zimmerman, R., Ohene-Frempong, K., Melhem, E.R., 2014. Sickle cell anemia: intracranial stenosis and silent cerebral infarcts in children with low risk of stroke. *Adv. Med. Sci.* 59, 108–113.
- Arteaga, D.F., Strother, M.K., Davis, L.T., Fusco, M.R., Faraco, C.C., Roach, B.A., Scott, A.O., Donahue, M.J., 2017. Planning-free cerebral blood flow territory mapping in patients with intracranial arterial stenosis. *J. Cereb. Blood Flow. Metab.* 37, 1944–1958.
- Ashkanian, M., Borghammer, P., Gjedde, A., Ostergaard, L., Vafaei, M., 2008. Improvement of brain tissue oxygenation by inhalation of carbogen. *Neuroscience* 156, 932–938.
- Attye, A., Villien, M., Tahon, F., Warnking, J., Detante, O., Krainik, A., 2014. Normalization of cerebral vasoreactivity using BOLD MRI after intravascular stenting. *Hum. Brain Mapp.* 35, 1320–1324.
- Balkaran, B., Char, G., Morris, J.S., Thomas, P.W., Serjeant, B.E., Serjeant, G.R., 1992. Stroke in a cohort of patients with homozygous sickle cell disease. *J. Pediatr.* 120, 360–366.
- Banerjee, C., Chimowitz, M.I., 2017. Stroke caused by atherosclerosis of the major intracranial arteries. *Circ. Res.* 120, 502–513.
- Baron, J.C., 2001. Perfusion thresholds in human cerebral ischemia: historical perspective and therapeutic implications. *Cerebrovasc Dis.* 11 (Suppl. 1), 2–8.
- Bhogal, A.A., Siero, J.C., Fisher, J.A., Froeling, M., Luijten, P., Philippens, M., Hoogduin, H., 2014. Investigating the non-linearity of the BOLD cerebrovascular reactivity response to targeted hypo/hypercapnia at 7T. *Neuroimage* 98, 296–305.
- Bhogal, A.A., Philippens, M.E., Siero, J.C., Fisher, J.A., Petersen, E.T., Luijten, P.R., Hoogduin, H., 2015. Examining the regional and cerebral depth-dependent BOLD cerebrovascular reactivity response at 7T. *Neuroimage* 114, 239–248.
- Bhogal, A.A., De Vis, J.B., Siero, J.C.W., Petersen, E.T., Luijten, P.R., Hendrikse, J., Philippens, M.E.P., Hoogduin, H., 2016. The BOLD cerebrovascular reactivity response to progressive hypercapnia in young and elderly. *Neuroimage* 139, 94–102.
- Blair, G.W., Doubal, F.N., Thrippleton, M.J., Marshall, I., Wardlaw, J.M., 2016. Magnetic resonance imaging for assessment of cerebrovascular reactivity in cerebral small vessel disease: a systematic review. *J. Cereb. Blood Flow. Metab.* 36, 833–841.
- Blicher, J.U., Stagg, C.J., O’Shea, J., Ostergaard, L., MacIntosh, B.J., Johansen-Berg, H., Jezzard, P., Donahue, M.J., 2012. Visualization of altered neurovascular coupling in chronic stroke patients using multimodal functional MRI. *J. Cereb. Blood Flow. Metab.* 32, 2044–2054.
- Blockley, N.P., Harkin, J.W., Bulte, D.P., 2017. Rapid cerebrovascular reactivity mapping: enabling vascular reactivity information to be routinely acquired. *Neuroimage* 159, 214–223.
- Boles Ponto, L.L., Schultz, S.K., Leonard Watkins, G., Hichwa, R.D., 2004. Technical issues in the determination of cerebrovascular reserve in elderly subjects using 15O-water PET imaging. *Neuroimage* 21, 201–210.
- Bonte, F.J., Devous, M.D., Reisch, J.S., 1988. The effect of acetazolamide on regional cerebral blood flow in normal human subjects as measured by single-photon emission computed tomography. *Invest. Radiol.* 23, 564–568.
- Bouvier, J., Detante, O., Tahon, F., Attye, A., Perret, T., Chechin, D., Baribeau, M., Boubagra, K., Garambois, K., Tropres, I., Grand, S., Barbier, E.L., Krainik, A., 2015. Reduced CMRO(2) and cerebrovascular reserve in patients with severe intracranial arterial stenosis: a combined multiparametric qBOLD oxygenation and BOLD fMRI study. *Hum. Brain Mapp.* 36, 695–706.
- Bright, M.G., Bulte, D.P., Jezzard, P., Duyn, J.H., 2009. Characterization of regional heterogeneity in cerebrovascular reactivity dynamics using novel hypoxia task and BOLD fMRI. *Neuroimage* 48, 166–175.
- Bulte, D., Chiarelli, P., Wise, R., Jezzard, P., 2007a. Measurement of cerebral blood volume in humans using hyperoxic MRI contrast. *J. Magn. Reson. Imaging* 26, 894–899.

- Bulte, D.P., Chiarelli, P.A., Wise, R.G., Jezzard, P., 2007b. Cerebral perfusion response to hyperoxia. *J. Cereb. Blood Flow. Metab.* 27, 69–75.
- Chollet, F., Celsis, P., Clanet, M., Guiraud-Chaumeil, B., Rascol, A., Marc-Vergnes, J.P., 1989. SPECT study of cerebral blood flow reactivity after acetazolamide in patients with transient ischemic attacks. *Stroke* 20, 458–464.
- Christen, T., Bolar, D.S., Zaharchuk, G., 2013. Imaging brain oxygenation with MRI using blood oxygenation approaches: methods, validation, and clinical applications. *AJNR Am. J. Neuroradiol.* 34, 1113–1123.
- Cipolla, M.J., 2009. The Cerebral Circulation. Morgan & Claypool Life Sciences, San Rafael.
- Cogswell, P.M., Davis, T.L., Strother, M.K., Faraco, C.C., Scott, A.O., Jordan, L.C., Fusco, M.R., Frederick, B.D., Hendrikse, J., Donahue, M.J., 2017 Oct. Impact of vessel wall lesions and vascular stenoses on cerebrovascular reactivity in patients with intracranial stenotic disease. *J. Magn. Reson Imaging* 46 (4), 1167–1176.
- Conijn, M.M., Hoogduin, J.M., van der Graaf, Y., Hendrikse, J., Luijten, P.R., Geerlings, M.I., 2012. Microbleeds, lacunar infarcts, white matter lesions and cerebrovascular reactivity – a 7 T study. *Neuroimage* 59, 950–956.
- de Boorder, M.J., Hendrikse, J., van der Grond, J., 2004. Phase-contrast magnetic resonance imaging measurements of cerebral autoregulation with a breath-hold challenge: a feasibility study. *Stroke* 35, 1350–1354.
- De Vis, J.B., Hendrikse, J., Bhogal, A., Adams, A., Kappelle, L.J., Petersen, E.T., 2015. Age-related changes in brain hemodynamics: A calibrated MRI study. *Hum. Brain Mapp.* 36, 3973–3987.
- Derdeyn, C.P., Grubb Jr., R.L., Powers, W.J., 1999. Cerebral hemodynamic impairment: methods of measurement and association with stroke risk. *Neurology* 53, 251–259.
- Derdeyn, C.P., Videen, T.O., Yundt, K.D., Fritsch, S.M., Carpenter, D.A., Grubb, R.L., Powers, W.J., 2002. Variability of cerebral blood volume and oxygen extraction: stages of cerebral haemodynamic impairment revisited. *Brain* 125, 595–607.
- Derdeyn, C.P., Chimowitz, M.I., Lynn, M.J., Fiorella, D., Turan, T.N., Janis, L.S., Montgomery, J., Nizam, A., Lane, B.F., Lutsep, H.L., Barnwell, S.L., Waters, M.F., Hoh, B.L., Hourihane, J.M., Levy, E.I., Alexandrov, A.V., Harrigan, M.R., Chiu, D., Klucznik, R.P., Clark, J.M., McDougall, C.G., Johnson, M.D., Pride Jr., G.L., Lynch, J.R., Zaidat, O.O., Rumboldt, Z., Cloft, H.J., Stenting, Aggressive Medical Management for Preventing Recurrent Stroke in Intracranial Stenosis Trial, I, 2014. Aggressive medical treatment with or without stenting in high-risk patients with intracranial artery stenosis (SAMMPRISS): the final results of a randomised trial. *Lancet* 383, 333–341.
- Dijkhuizen, R.M., Zaharchuk, G., Otte, W.M., 2014. Assessment and modulation of resting-state neural networks after stroke. *Curr. Opin. Neurol.* 27, 637–643.
- Donahue, M.J., Stevens, R.D., de Boorder, M., Pekar, J.J., Hendrikse, J., van Zijl, P.C., 2009. Hemodynamic changes after visual stimulation and breath holding provide evidence for an uncoupling of cerebral blood flow and volume from oxygen metabolism. *J. Cereb. Blood Flow. Metab.* 29, 176–185.
- Donahue, M.J., Hoogduin, H., van Zijl, P.C., Jezzard, P., Luijten, P.R., Hendrikse, J., 2011. Blood oxygenation level-dependent (BOLD) total and extravascular signal changes and DeltaR2\* in human visual cortex at 1.5, 3.0 and 7.0 T. *NMR Biomed.* 24, 25–34.
- Donahue, M.J., Strother, M.K., Hendrikse, J., 2012. Novel MRI approaches for assessing cerebral hemodynamics in ischemic cerebrovascular disease. *Stroke* 43, 903–915.
- Donahue, M.J., Ayad, M., Moore, R., van Osch, M., Singer, R., Clemons, P., Strother, M., 2013. Relationships between hypercarbic reactivity, cerebral blood flow, and arterial circulation times in patients with moyamoya disease. *J. Magn. Reson Imaging* 38, 1129–1139. *Epublish ahead of print.*
- Donahue, M.J., Dethrage, L.M., Faraco, C.C., Jordan, L.C., Clemons, P., Singer, R., Mocco, J., Shyr, Y., Desai, A., O'Duffy, A., Riebau, D., Hermann, L., Connors, J., Kirshner, H., Strother, M.K., 2014a. Routine clinical evaluation of cerebrovascular reserve capacity using carbogen in patients with intracranial stenosis. *Stroke* 45, 2335–2341.
- Donahue, M.J., Faraco, C.C., Strother, M.K., Chappell, M.A., Rane, S., Dethrage, L.M., Hendrikse, J., Siero, J.C., 2014b. Bolus arrival time and cerebral blood flow responses to hypercarbia. *J. Cereb. Blood Flow. Metab.* 34, 1243–1252.
- Donahue, M.J., Strother, M.K., L., Hocke, L.M., Tong, Y., Frederick, B., 2015. Time delay processing of hypercapnic fMRI allows quantitative parameterization of cerebrovascular reactivity and blood flow delays. *J. Cereb. Blood Flow. Metab.* 36, 1767–1779.
- Donahue, M.J., Juttukonda, M.R., Watchmaker, J.M., 2016a. Noise concerns and post-processing procedures in cerebral blood flow (CBF) and cerebral blood volume (CBV) functional magnetic resonance imaging. *Neuroimage* 154, 43–58.
- Donahue, M.J., Strother, M.K., Lindsey, K.P., Hocke, L.M., Tong, Y., Frederick, B.D., 2016b. Time delay processing of hypercapnic fMRI allows quantitative parameterization of cerebrovascular reactivity and blood flow delays. *J. Cereb. Blood Flow. Metab.* 36, 1767–1779.
- Donahue, M.J., Achten, E., Cogswell, P.M., De Leeuw, F.E., Derdeyn, C.P., Dijkhuizen, R.M., Fan, A.P., Ghaznawi, R., Heit, J.J., Ikram, M.A., Jezzard, P., Jordan, L.C., Jouvent, E., Knutsson, L., Leigh, R., Liebeskind, D.S., Lin, W., Okell, T.W., Qureshi, A.I., Stagg, C.J., van Osch, M.J., van Zijl, P.C., Watchmaker, J.M., Wintermark, M., Wu, O., Zaharchuk, G., Zhou, J., Hendrikse, J., 2017a. Consensus statement on current and emerging methods for the diagnosis and evaluation of cerebrovascular disease. *J. Cereb. Blood Flow. Metab.* 271678X17721830, *Epublish ahead of print.*
- Donahue, M.J., Juttukonda, M.R., Watchmaker, J.M., 2017b. Noise concerns and post-processing procedures in cerebral blood flow (CBF) and cerebral blood volume (CBV) functional magnetic resonance imaging. *Neuroimage* 154, 43–58.
- Duong, T.Q., Yacob, E., Adriany, G., Hu, X., Ugurbil, K., Kim, S.G., 2003. Microvascular BOLD contribution at 4 and 7 T in the human brain: gradient-echo and spin-echo fMRI with suppression of blood effects. *Magn. Reson Med.* 49, 1019–1027.
- Enzmann, D.R., Pelc, N.J., 1991. Normal flow patterns of intracranial and spinal cerebrospinal fluid defined with phase-contrast cine MR imaging. *Radiology* 178, 467–474.
- Enzmann, D.R., Ross, M.R., Marks, M.P., Pelc, N.J., 1994. Blood flow in major cerebral arteries measured by phase-contrast cine MR. *AJNR Am. J. Neuroradiol.* 15, 123–129.
- Famakin, B.M., Chimowitz, M.I., Lynn, M.J., Stern, B.J., George, M.G., 2009. Causes and severity of ischemic stroke in patients with symptomatic intracranial arterial stenosis. *Stroke. a J. Cereb. Circ.* 40, 1999–2003.
- Fan, A.P., Guo, J., Khalighi, M.M., Gulaka, P.K., Shen, B., Park, J.H., Gandhi, H., Holley, D., Rutledge, O., Singh, P., Haywood, T., Steinberg, G.K., Chin, F.T., Zaharchuk, G., 2017. Long-delay arterial spin labeling provides more accurate cerebral blood flow measurements in moyamoya patients: a simultaneous positron emission tomography/MRI study. *Stroke* 48, 2441–2449.
- Faraco, C.C., Strother, M.K., Siero, J.C., Arteaga, D.F., Scott, A.O., Jordan, L.C., Donahue, M.J., 2015. The cumulative influence of hyperoxia and hypercapnia on blood oxygenation and R. *J. Cereb. Blood Flow. Metab.* 35, 203–2042.
- Federau, C., Christensen, S., Zun, Z., Park, S.W., Ni, W., Moseley, M., Zaharchuk, G., 2017. Cerebral blood flow, transit time, and apparent diffusion coefficient in moyamoya disease before and after acetazolamide. *Neuroradiology* 59, 5–12.
- Fernandez-Seara, M.A., Techawiboonwong, A., Detre, J.A., Wehrli, F.W., 2006. MR susceptibility for measuring global brain oxygen extraction. *Magn. Reson Med.* 55, 967–973.
- Fierstra, J., Sobczyk, O., Battisti-Charbonney, A., Mandell, D.M., Poublanc, J., Crawley, A.P., Mikulis, D.J., Duffin, J., Fisher, J.A., 2013. Measuring cerebrovascular reactivity: what stimulus to use? *J. Physiol.* 591, 5809–5821.
- Filosa, J.A., Morrison, H.W., Iddings, J.A., Du, W., Kim, K.J., 2016. Beyond neurovascular coupling, role of astrocytes in the regulation of vascular tone. *Neuroscience* 323, 96–109.
- Fisher, J.A., Sobczyk, O., Crawley, A., Poublanc, J., Dufort, P., Venkatraghavan, L., Sam, K., Mikulis, D., Duffin, J., 2017. Assessing cerebrovascular reactivity by the pattern of response to progressive hypercapnia. *Hum. Brain Mapp. (Epublish ahead of print)*.
- Gevers, S., Nederveen, A.J., Fijnvandraat, K., van den Berg, S.M., van Ooij, P., Heijtel, D.F., Heijboer, H., Nederkoorn, P.J., Engelen, M., van Osch, M.J., Majoi, C.B., 2012. Arterial spin labeling measurement of cerebral perfusion in children with sickle cell disease. *J. Magn. Reson Imaging* 35, 779–787.
- Goldstein, L.B., American Heart Association., American Stroke Association, 2009. A Primer on Stroke Prevention and Treatment : an Overview Based on AHA/ASA Guidelines. Wiley-Blackwell, Chichester, UK; Hoboken, NJ.
- Golestanian, A.M., Wei, L.L., Chen, J.J., 2016. Quantitative mapping of cerebrovascular reactivity using resting-state BOLD fMRI: validation in healthy adults. *Neuroimage* 138, 147–163.
- González, R.G., 2005. Acute Ischemic Stroke: Imaging and Intervention. Springer, Berlin; New York.
- Goode, S.D., Altaf, N., Munshi, S., MacSweeney, S.T., Auer, D.P., 2016. Impaired cerebrovascular reactivity predicts recurrent symptoms in patients with carotid artery occlusion: a hypercapnia BOLD fMRI study. *AJNR Am. J. Neuroradiol.* 37, 904–909.
- Grubb Jr., R.L., Derdeyn, C.P., Fritsch, S.M., Carpenter, D.A., Yundt, K.D., Videen, T.O., Spitznagel, E.L., Powers, W.J., 1998. Importance of hemodynamic factors in the prognosis of symptomatic carotid occlusion. *JAMA* 280, 1055–1060.
- Gunther, M., Oshio, K., Feinberg, D.A., 2005. Single-shot 3D imaging techniques improve arterial spin labeling perfusion measurements. *Magn. Reson Med.* 54, 491–498.
- Guppy, K.H., Charbel, F.T., Corsten, L.A., Zhao, M., Debrun, G., 2002. Hemodynamic evaluation of basilar and vertebral artery angioplasty. *Neurosurgery* 51, 327–333 discussion 333–324.
- Gupta, A., Chazen, J.L., Hartman, M., Delgado, D., Anumula, N., Shao, H., Mazumdar, M., Segal, A.Z., Kamel, H., Leifer, D., Sanelli, P.C., 2012. Cerebrovascular reserve and stroke risk in patients with carotid stenosis or occlusion: a systematic review and meta-analysis. *Stroke* 43, 2884–2891.
- Guyton, A.C., 1977. Basic Human Physiology: Normal Function and Mechanisms of Disease, 2d ed. Saunders, Philadelphia.
- Guyton, A.C., Hall, J.E., 2006. Textbook of Medical Physiology, eleventh ed. Elsevier Saunders, Philadelphia.
- Hallemeier, C.L., Rich, K.M., Grubb Jr., R.L., Chicoine, M.R., Moran, C.J., Cross 3rd, D.T., Zipfel, G.J., Dacey Jr., R.G., Derdeyn, C.P., 2006. Clinical features and outcome in North American adults with moyamoya phenomenon. *Stroke* 37, 1490–1496.
- Harder, D.R., Madden, J.A., 1985. Cellular mechanism of force development in cat middle cerebral artery by reduced PCO2. *Pflugers Arch.* 403, 402–406.
- Hashimoto, A., Mikami, T., Komatsu, K., Noshiro, S., Hirano, T., Wanibuchi, M., Mikuni, N., 2017. Assessment of hemodynamic compromise using computed tomography perfusion in combination with 123I-IMP single-photon emission computed tomography without acetazolamide challenge test. *J. Stroke Cerebrovasc. Dis.* 26, 627–635.
- Hawkins, B.T., Davis, T.P., 2005. The blood-brain barrier/neurovascular unit in health and disease. *Pharmacol. Rev.* 57, 173–185.
- Hendrikse, J., van Raam, A.F., van der Graaf, Y., Mali, W.P., van der Grond, J., 2005. Distribution of cerebral blood flow in the circle of Willis. *Radiology* 235, 184–189.
- Hoshi, H., Ohnishi, T., Jinnouchi, S., Futami, S., Nagamachi, S., Kodama, T., Watanabe, K., Ueda, T., Wakisaka, S., 1994. Cerebral blood flow study in patients with moyamoya disease evaluated by IMP SPECT. *J. Nucl. Med.* 35, 44–50.
- Hsu, B., 2013. PET tracers and techniques for measuring myocardial blood flow in patients with coronary artery disease. *J. Biomed. Res.* 27, 452–459.
- Huber, L., Goense, J., Kennerley, A.J., Ivanov, D., Krieger, S.N., Lepsiens, J., Trampel, R., Turner, R., Moller, H.E., 2014. Investigation of the neurovascular coupling in positive and negative BOLD responses in human brain at 7 T. *Neuroimage* 97, 349–362.

- Huber, L., Goense, J., Kennerley, A., Guidi, M., Trampel, R., Turner, R., Moller, H.E., 2015. Micro- and Macrovascular Contributions to Layer-dependent Blood Volume FMRI: a Multi-modal, Multi-species Comparison. 23rd Annual International Society for Magnetic Resonance in Medicine, Toronto, Canada, p. 317.
- Hund-Georgiadis, M., Zysset, S., Naganawa, S., Norris, D.G., Von Cramon, D.Y., 2003. Determination of cerebrovascular reactivity by means of fMRI signal changes in cerebral microangiopathy: a correlation with morphological abnormalities. *Cerebrovasc. Dis.* 16, 158–165.
- Hurlet-Jensen, A.M., Prohovnik, I., Pavlakis, S.G., Piomelli, S., 1994. Effects of total hemoglobin and hemoglobin S concentration on cerebral blood flow during transfusion therapy to prevent stroke in sickle cell disease. *Stroke* 25, 1688–1692.
- Ikezaki, K., 2000. Rational approach to treatment of moyamoya disease in childhood. *J. Child. Neurol.* 15, 350–356.
- Itada, N., Forster, R.E., 1977. Carbonic anhydrase activity in intact red blood cells measured with  $^{180}$  exchange. *J. Biol. Chem.* 252, 3881–3890.
- Itoh, Y., Suzuki, N., 2012. Control of brain capillary blood flow. *J. Cereb. Blood Flow. Metab.* 32, 1167–1176.
- Jahanian, H., Christen, T., Moseley, M.E., Pajewski, N.M., Wright, C.B., Tamura, M.K., Zaharchuk, G., Group, S.S.R., 2017. Measuring vascular reactivity with resting-state blood oxygenation level-dependent (BOLD) signal fluctuations: a potential alternative to the breath-holding challenge? *J. Cereb. Blood Flow. Metab.* 37, 2526–2538.
- Jordan, L.C., Gindville, M.C., Scott, A.O., Juttukonda, M.R., Strother, M.K., Kassim, A.A., Chen, S.C., Lu, H., Pruthi, S., Shyr, Y., Donahue, M.J., 2016. Non-invasive imaging of oxygen extraction fraction in adults with sickle cell anaemia. *Brain* 139, 738–750.
- Kasner, S.E., Gorelick, P.B., 2004. Prevention and Treatment of Ischemic Stroke. Butterworth-Heinemann, Philadelphia.
- Kassim, A.A., DeBaun, M.R., 2013. Sickle cell disease, vasculopathy, and therapeutics. *Annu. Rev. Med.* 64, 451–466.
- Kawabori, M., Kuroda, S., Nakayama, N., Hirata, K., Shiga, T., Houkin, K., Tamaki, N., 2013. Effective surgical revascularization improves cerebral hemodynamics and resolves headache in pediatric Moyamoya disease. *World Neurosurg.* 80, 612–619.
- Kennedy, C., Sokoloff, L., 1957. An adaptation of the nitrous oxide method to the study of the cerebral circulation in children; normal values for cerebral blood flow and cerebral metabolic rate in childhood. *J. Clin. Invest* 36, 1130–1137.
- Kety, S.S., Schmidt, C.F., 1948. The effects of altered arterial tensions of carbon dioxide and oxygen on cerebral blood flow and cerebral oxygen consumption of normal young men. *J. Clin. Invest* 27, 484–492.
- Kim, K.J., Filosa, J.A., 2012. Advanced in vitro approach to study neurovascular coupling mechanisms in the brain microcirculation. *J. Physiol.* 590, 1757–1770.
- Kim, Y.C., Lee, S.J., Kim, K.W., 2004. Effects of pH on vascular tone in rabbit basilar arteries. *J. Korean Med. Sci.* 19, 42–50.
- Kim, J.A., Leung, J., Lerch, J.P., Kassner, A., 2016. Reduced cerebrovascular reserve is regionally associated with cortical thickness reductions in children with sickle cell disease. *Brain Res.* 1642, 263–269.
- Kleiser, B., Widder, B., 1992. Course of carotid artery occlusions with impaired cerebrovascular reactivity. *Stroke* 23, 171–174.
- Klockner, U., Isenberg, G., 1994. Calcium channel current of vascular smooth muscle cells: extracellular protons modulate gating and single channel conductance. *J. Gen. Physiol.* 103, 665–678.
- Koller, A., Toth, P., 2012. Contribution of flow-dependent vasomotor mechanisms to the autoregulation of cerebral blood flow. *J. Vasc. Res.* 49, 375–389.
- Kontos, H.A., Raper, A.J., Patterson, J.L., 1977. Analysis of vasoactivity of local pH, PCO<sub>2</sub> and bicarbonate on pial vessels. *Stroke* 8, 358–360.
- Kosinski, P.D., Croal, P.L., Leung, J., Williams, S., Odame, I., Hare, G.M., Shroff, M., Kassner, A., 2017. The severity of anaemia depletes cerebrovascular dilatory reserve in children with sickle cell disease: a quantitative magnetic resonance imaging study. *Br. J. Haematol.* 176, 280–287.
- Ladner, T.R., Donahue, M.J., Arteaga, D.F., Faraco, C.C., Roach, B.A., Davis, L.T., Jordan, L.C., Froehler, M.T., Strother, M.K., 2017. Prior Infarcts, Reactivity, and Angiography in Moyamoya Disease (PIRAMD): a scoring system for moyamoya severity based on multimodal hemodynamic imaging. *J. Neurosurg.* 126, 495–503.
- Lee, J.M., Vo, K.D., An, H., Celik, A., Lee, Y., Hsu, C.Y., Lin, W., 2003. Magnetic resonance cerebral metabolic rate of oxygen utilization in hyperacute stroke patients. *Ann. Neurol.* 53, 227–232.
- Leenders, K.L., Perani, D., Lammertsma, A.A., Heather, J.D., Buckingham, P., Healy, M.J., Gibbs, J.M., Wise, R.J., Hatazawa, J., Herold, S., et al., 1990. Cerebral blood flow, blood volume and oxygen utilization. Normal values and effect of age. *Brain* 113 (Pt 1), 27–47.
- Leigh, R., Knutsson, L., Zhou, J., van Zijl, P.C., 2017. Imaging the physiological evolution of the ischemic penumbra in acute ischemic stroke. *J. Cereb. Blood Flow. Metab.* 271678X17700913, Epub ahead of print.
- Liebeskind, D.S., Cotsonis, G.A., Saver, J.L., Lynn, M.J., Turan, T.N., Cloft, H.J., Chimowitz, M.I., 2010. Collaterals dramatically alter stroke risk in intracranial atherosclerosis. *Ann. neurology* 69, 963–974.
- Lin, W., An, H., Ford, A.L., Chen, Y., Vo, K.D., Powers, W.J., Lee, J.M., 2013. MR imaging of oxygen extraction and neurovascular coupling. *Stroke* 44, S61–S64.
- Li, P., Li, Y., Pinho, M., Park, D.C., Welch, B.G., Lu, H., 2017a. Cerebrovascular reactivity mapping without gas challenges. *Neuroimage* 146, 320–326.
- Li, P., Welch, B.G., Li, Y., Gu, H., King, D., Yang, Y., Pinho, M., Lu, H., 2017b. Multiparametric imaging of brain hemodynamics and function using gas-inhalation MRI. *Neuroimage* 146, 715–723.
- Low, S.W., Teo, K., Lwin, S., Yeo, L.L., Paliwal, P.R., Ahmad, A., Sinha, A.K., Teoh, H.L., Wong, L.Y., Chong, V.F., Seet, R.C., Chan, B.P., Yeo, T.T., Chou, N., Sharma, V.K., 2015. Improvement in cerebral hemodynamic parameters and outcomes after superficial temporal artery-middle cerebral artery bypass in patients with severe stenoocclusive disease of the intracranial internal carotid or middle cerebral arteries. *J. Neurosurg.* 123, 662–669.
- Lu, H., Ge, Y., 2008. Quantitative evaluation of oxygenation in venous vessels using T<sub>2</sub>-Relaxation-Under-Spin-Tagging MRI. *Magn. Reson. Med.* 60, 357–363.
- Lu, H., Clingman, C., Golay, X., van Zijl, P.C., 2004. Determining the longitudinal relaxation time ( $T_1$ ) of blood at 3.0 Tesla. *Magn. Reson. Med.* 52, 679–682.
- Lu, H., Xu, F., Rodrigue, K.M., Kennedy, K.M., Cheng, Y., Flicker, B., Hebrank, A.C., Uh, J., Park, D.C., 2011. Alterations in cerebral metabolic rate and blood supply across the adult lifespan. *Cereb. Cortex* 21, 1426–1434.
- Ma, J., Mehrkens, J.H., Holtmannspötter, M., Linke, R., Schmid-Elsaesser, R., Steiger, H.J., Brueckmann, H., Bruening, R., 2007. Perfusion MRI before and after acetazolamide administration for assessment of cerebrovascular reserve capacity in patients with symptomatic internal carotid artery (ICA) occlusion: comparison with  $^{99m}$ Tc-ECD SPECT. *Neuroradiology* 49, 317–326.
- Mandell, D.M., Han, J.S., Poublanc, J., Crawley, A.P., Fierstra, J., Tymianski, M., Fisher, J.A., Mikulis, D.J., 2011. Quantitative measurement of cerebrovascular reactivity by blood oxygen level-dependent MR imaging in patients with intracranial stenosis: preoperative cerebrovascular reactivity predicts the effect of extracranial-intracranial bypass surgery. *AJNR Am. J. Neuroradiol.* 32, 721–727.
- Marstrand, J.R., Rostrup, E., Rosenbaum, S., Garde, E., Larsson, H.B., 2001. Cerebral hemodynamic changes measured by gradient-echo or spin-echo bolus tracking and its correlation to changes in ICA blood flow measured by phase-mapping MRI. *J. Magn. Reson Imaging* 14, 391–400.
- Masdeu, J.C., Brass, L.M., 1995. SPECT imaging of stroke. *J. Neuroimaging* 5 (Suppl. 1), S14–S22.
- Merola, A., Murphy, K., Stone, A.J., Germuska, M.A., Griffeth, V.E.M., Blockley, N.P., Buxton, R.B., Wise, R.G., 2016. Measurement of oxygen extraction fraction (OEF): an optimized BOLD signal model for use with hypercapnic and hyperoxic calibration. *Neuroimage* 129, 159–174.
- Moreton, F.C., Dani, K.A., Goutcher, C., O'Hare, K., Muir, K.W., 2016. Respiratory challenge MRI: practical aspects. *Neuroimage Clin.* 11, 667–677.
- Nagata, K., Yamazaki, T., Takano, D., Maeda, T., Fujimaki, Y., Nakase, T., Sato, Y., 2016. Cerebral circulation in aging. *Ageing Res. Rev.* 30, 49–60.
- Ohene-Frempong, K., Weiner, S.J., Sleeper, L.A., Miller, S.T., Embury, S., Moehr, J.W., Wethers, D.L., Pegelow, C.H., Gill, F.M., 1998. Cerebrovascular accidents in sickle cell disease: rates and risk factors. *Blood* 91, 288–294.
- Okell, T.W., Chappell, M.A., Kelly, M.E., Jezzard, P., 2013. Cerebral blood flow quantification using vessel-encoded arterial spin labeling. *J. Cereb. Blood Flow. Metab.* 33, 1716–1724.
- Oktar, S.O., Yucel, C., Karaosmanoglu, D., Akkan, K., Ozdemir, H., Tokgoz, N., Tali, T., 2006. Blood-flow volume quantification in internal carotid and vertebral arteries: comparison of 3 different ultrasound techniques with phase-contrast MR imaging. *AJNR Am. J. Neuroradiol.* 27, 363–369.
- Ovbiagele, B., Cruz-Flores, S., Lynn, M.J., Chimowitz, M.I., 2008. Early stroke risk after transient ischemic attack among individuals with symptomatic intracranial artery stenosis. *Arch. neurology* 65, 733–737.
- Patrick, J.T., Fritz, J.V., Adamo, J.M., Dandonna, P., 1996. Phase-contrast magnetic resonance angiography for the determination of cerebrovascular reserve. *J. Neuroimaging* 6, 137–143.
- Peng, S.L., Ravi, H., Sheng, M., Thomas, B.P., Lu, H., 2017. Searching for a truly “isometabolic” gas challenge in physiological MRI. *J. Cereb. Blood Flow. Metab.* 37, 715–725.
- Phi, J.H., Wang, K.C., Lee, J.Y., Kim, S.K., 2015. Moyamoya syndrome: a window of moyamoya disease. *J. Korean Neurosurg. Soc.* 57, 408–414.
- Piechnik, S.K., Chiarelli, P.A., Jezzard, P., 2008. Modelling vascular reactivity to investigate the basis of the relationship between cerebral blood volume and flow under CO<sub>2</sub> manipulation. *Neuroimage* 39, 107–118.
- Pindzola, R.R., Balzer, J.R., Nemoto, E.M., Goldstein, S., Yonas, H., 2001. Cerebrovascular reserve in patients with carotid occlusive disease assessed by stable xenon-enhanced CT cerebral blood flow and transcranial Doppler. *Stroke* 32, 1811–1817.
- Pinto, J., Jorge, J., Sousa, I., Vilela, P., Figueiredo, P., 2016. Fourier modeling of the BOLD response to a breath-hold task: optimization and reproducibility. *Neuroimage* 135, 223–231.
- Platt, D., Griggs, R.C., 2012. Use of acetazolamide in sulfonamide-allergic patients with neurologic channelopathies. *Arch. Neurol.* 69, 527–529.
- Powers, W.J., 1991. Cerebral hemodynamics in ischemic cerebrovascular disease. *Ann. Neurol.* 29, 231–240.
- Prohovnik, I., Hurlet-Jensen, A., Adams, R., De Vivo, D., Pavlakis, S.G., 2009. Hemodynamic etiology of elevated flow velocity and stroke in sickle-cell disease. *J. Cereb. Blood Flow. Metab.* 29, 803–810.
- Prokopiou, P.C., Murphy, K., Wise, R.G., Mitsis, G.D., 2016. Estimation of voxel-wise dynamic cerebrovascular reactivity curves from resting-state fMRI data. *Conf. Proc. IEEE Eng. Med. Biol. Soc.* 2016, 1143–1146.
- Purves, D., Williams, S.M., 2001. Neuroscience, second ed. Sinauer Associates, Sunderland, Mass.
- Rane, S.D., Gore, J.C., 2013. Measurement of  $T_1$  of human arterial and venous blood at 7T. *Magn. Reson. Imaging* 31, 477–479.
- Rane, S., Mason, E., Hussey, E., Gore, J., Ally, B.A., Donahue, M.J., 2014. The effect of echo time and post-processing procedure on blood oxygenation level-dependent (BOLD) functional connectivity analysis. *Neuroimage* 95, 39–47.
- Rapela, C.E., Green, H.D., 1964. Autoregulation of canine cerebral blood flow. *Circ. Res.* 15 (Suppl. I), 205–212.
- Ravi, H., Liu, P., Peng, S.L., Liu, H., Lu, H., 2016. Simultaneous multi-slice (SMS) acquisition enhances the sensitivity of hemodynamic mapping using gas challenges. *NMR Biomed.* 29, 1511–1518.

- Reed, A.B., Gaccione, P., Belkin, M., Donaldson, M.C., Mannick, J.A., Whittemore, A.D., Conte, M.S., 2003. Preoperative risk factors for carotid endarterectomy: defining the patient at high risk. *J. Vasc. Surg.* 37, 1191–1199.
- Roach, B.A., Donahue, M.J., Faraco, C.C., Artega, D.A., Davis, T.L., Scott, A.O., Strother, M.K., 2015. In: Interrogating the Functional Correlates of Collateralization in Patients with Intracranial Stenosis Using Multi-modal ASNR 53rd Annual Meeting & Symposium, Chicago, IL.
- Sam, K., Poublanc, J., Sobczyk, O., Han, J.S., Battisti-Charbonney, A., Mandell, D.M., Tymianski, M., Crawley, A.P., Fisher, J.A., Mikulis, D.J., 2015. Assessing the effect of unilateral cerebral revascularisation on the vascular reactivity of the non-intervened hemisphere: a retrospective observational study. *BMJ Open* 5, e006014.
- Sam, K., Crawley, A.P., Conklin, J., Poublanc, J., Sobczyk, O., Mandell, D.M., Venkatraghavan, L., Duffin, J., Fisher, J.A., Black, S.E., Mikulis, D.J., 2016. Development of white matter hyperintensity is preceded by reduced cerebrovascular reactivity. *Ann. Neurol.* 80, 277–285.
- SAMMPRISS, 2011. Stenting vs. Aggressive Medical Management for Preventing Recurrent Stroke in Intracranial Stenosis (SAMMPRISS). Medical University of South Carolina NIH NINDS.
- Scott, R.M., 2000. Moyamoya syndrome: a surgically treatable cause of stroke in the pediatric patient. *Clin. Neurosurg.* 47, 378–384.
- Scott, R.M., Smith, E.R., 2009. Moyamoya disease and moyamoya syndrome. *N. Engl. J. Med.* 360, 1226–1237.
- Scott, R.M., Smith, J.L., Robertson, R.L., Madsen, J.R., Soriano, S.G., Rockoff, M.A., 2004. Long-term outcome in children with moyamoya syndrome after cranial revascularization by pial synangiosis. *J. Neurosurg.* 100, 142–149.
- Settakits, G., Molnar, C., Kerenyi, L., Kollar, J., Legemate, D., Csiba, L., Fulesdi, B., 2003. Acetazolamide as a vasodilatory stimulus in cerebrovascular diseases and in conditions affecting the cerebral vasculature. *Eur. J. Neurol.* 10, 609–620.
- Siero, J.C., Hendrikse, J., Hoogduin, H., Petridou, N., Luijten, P., Donahue, M.J., 2015a. Cortical depth dependence of the BOLD initial dip and poststimulus undershoot in human visual cortex at 7 Tesla. *Magn. Reson Med.* 73, 2283–2295.
- Siero, J.C., Strother, M.K., Faraco, C.C., Hoogduin, H., Hendrikse, J., Donahue, M.J., 2015b. In vivo quantification of hyperoxic arterial blood water  $T_1$ . *NMR Biomed.* 28, 1518–1525.
- Silvestrini, M., Vernieri, F., Pasqualetti, P., Matteis, M., Passarelli, F., Troisi, E., Caltagirone, C., 2000. Impaired cerebral vasoreactivity and risk of stroke in patients with asymptomatic carotid artery stenosis. *JAMA* 283, 2122–2127.
- Smeeling, D.P., Hendrikse, J., Petersen, E.T., Donahue, M.J., de Vis, J.B., 2016. Arterial spin labeling and blood oxygen level-dependent MRI cerebrovascular reactivity in cerebrovascular disease: a systematic review and meta-analysis. *Cerebrovasc. Dis.* 42, 288–307.
- Spano, V.R., Mandell, D.M., Poublanc, J., Sam, K., Battisti-Charbonney, A., Pucci, O., Han, J.S., Crawley, A.P., Fisher, J.A., Mikulis, D.J., 2013. CO<sub>2</sub> blood oxygen level-dependent MR mapping of cerebrovascular reserve in a clinical population: safety, tolerability, and technical feasibility. *Radiology* 266, 592–598.
- Splitt, A., Box, F.M., van der Geest, R.J., Reiber, J.H., Kunz, P., Kamper, A.M., Blauw, G.J., van Buchem, M.A., 2002. Reproducibility of total cerebral blood flow measurements using phase contrast magnetic resonance imaging. *J. Magn. Reson Imaging* 16, 1–5.
- Strouse, J.J., Jordan, L.C., Lanzkron, S., Casella, J.F., 2009. The excess burden of stroke in hospitalized adults with sickle cell disease. *Am. J. Hematol.* 84, 548–552.
- Suga, Y., Ogasawara, K., Saito, H., Komoribayashi, N., Kobayashi, M., Inoue, T., Otawara, Y., Ogawa, A., 2007. Preoperative cerebral hemodynamic impairment and reactive oxygen species produced during carotid endarterectomy correlate with development of postoperative cerebral hyperperfusion. *Stroke* 38, 2712–2717.
- Swenson, E.R., 2014. New insights into carbonic anhydrase inhibition, vasodilation, and treatment of hypertensive-related diseases. *Curr. Hypertens. Rep.* 16, 467.
- Tancredi, F.B., Lajoie, I., Hoge, R.D., 2014. A simple breathing circuit allowing precise control of inspiratory gases for experimental respiratory manipulations. *BMC Res. Notes* 7, 235.
- Tancredi, F.B., Lajoie, I., Hoge, R.D., 2015. Test-retest reliability of cerebral blood flow and blood oxygenation level-dependent responses to hypercapnia and hyperoxia using dual-echo pseudo-continuous arterial spin labeling and step changes in the fractional composition of inspired gases. *J. Magn. Reson Imaging* 42, 1144–1157.
- Tatemichi, T.K., Prohovnik, I., Mohr, J.P., Correll, J.W., Quest, D.O., Jarvis, L., 1988. Reduced hypercapnic vasoreactivity in moyamoya disease. *Neurology* 38, 1575–1581.
- Telischak, N.A., Detre, J.A., Zaharchuk, G., 2015. Arterial spin labeling MRI: clinical applications in the brain. *J. Magn. Reson Imaging* 41, 1165–1180.
- Ter-Pogossian, M.M., Herscovitch, P., 1985. Radioactive oxygen-15 in the study of cerebral blood flow, blood volume, and oxygen metabolism. *Semin. Nucl. Med.* 15, 377–394.
- Thomas, B.P., Liu, P., Park, D.C., van Osch, M.J., Lu, H., 2014. Cerebrovascular reactivity in the brain white matter: magnitude, temporal characteristics, and age effects. *J. Cereb. Blood Flow. Metab.* 34, 242–247.
- Tong, Y., Frederick, B.D., 2014. Studying the spatial distribution of physiological effects on BOLD signals using ultrafast fMRI. *Front. Hum. Neurosci.* 8, 196.
- Triantafyllou, C., Hoge, R.D., Krueger, G., Wiggins, C.J., Potthast, A., Wiggins, G.C., Wald, L.L., 2005. Comparison of physiological noise at 1.5 T, 3 T and 7 T and optimization of fMRI acquisition parameters. *Neuroimage* 26, 243–250.
- Urback, A.L., MacIntosh, B.J., Goldstein, B.I., 2017. Cerebrovascular reactivity measured by functional magnetic resonance imaging during breath-hold challenge: a systematic review. *Neurosci. Biobehav. Rev.* 79, 27–47.
- Václavů, L., van der Land, V., Heijtel, D.F., van Osch, M.J., Cnossen, M.H., Majoie, C.B., Bush, A., Wood, J.C., Fijnvandraat, K.J., Mutsaerts, H.J., Nederveen, A.J., 2016. In vivo  $T_1$  of blood measurements in children with sickle cell disease improve cerebral blood flow quantification from arterial spin-labeling MRI. *AJR Am. J. Neuroradiol.* 37, 1727–1732.
- Václavů, L., Meynard, B., Mutsaerts, J., Petersen, E.T., Biemond, B., Nederveen, A.J., 2017. Dynamic cerebrovascular reactivity mapping in sickle cell disease using pCASL with acetazolamide administration. In: 3rd International Symposium on Imaging Cerebral Physiology, Cardiff, Wales.
- van Zijl, P.C., Eleff, S.M., Ulatowski, J.A., Oja, J.M., Ulug, A.M., Traystman, R.J., Kauppinen, R.A., 1998. Quantitative assessment of blood flow, blood volume and blood oxygenation effects in functional magnetic resonance imaging. *Nat. Med.* 4, 159–167.
- Vermier, F., Pasqualetti, P., Passarelli, F., Rossini, P.M., Silvestrini, M., 1999. Outcome of carotid artery occlusion is predicted by cerebrovascular reactivity. *Stroke* 30, 593–598.
- Voeks, J.H., Howard, G., Roubin, G.S., Malas, M.B., Cohen, D.J., Sternbergh 3rd, W.C., Aronow, H.D., Eskandari, M.K., Sheffet, A.J., Lal, B.K., Meschia, J.F., Brott, T.G., 2011. Age and outcomes after carotid stenting and endarterectomy: the carotid revascularization endarterectomy versus stenting trial. *Stroke; a J. Cereb. Circ.* 42, 3484–3490.
- Vorstrup, S., Lass, P., Waldemar, G., Brandi, L., Schmidt, J.F., Johnsen, A., Paulson, O.B., 1992. Increased cerebral blood flow in anemic patients on long-term hemodialytic treatment. *J. Cereb. Blood Flow. Metab.* 12, 745–749.
- Vrselja, Z., Brkic, H., Mrdenovic, S., Radic, R., Curic, G., 2014. Function of circle of Willis. *J. Cereb. Blood Flow. Metab.* 34, 578–584.
- Wardlaw, J.M., Smith, C., Dichgans, M., 2013a. Mechanisms of sporadic cerebral small vessel disease: insights from neuroimaging. *Lancet Neurol.* 12, 483–497.
- Wardlaw, J.M., Smith, E.E., Biessels, G.J., Cordonnier, C., Fazekas, F., Frayne, R., Lindley, R.I., O'Brien, J.T., Barkhof, F., Benavente, O.R., Black, S.E., Brayne, C., Breteler, M., Chabriat, H., Decarli, C., de Leeuw, F.E., Doubal, F., Duering, M., Fox, N.C., Greenberg, S., Hachinski, V., Kilmann, I., Mok, V., Oostenbrugge, R., Pantoni, L., Speck, O., Stephan, B.C., Teipel, S., Viswanathan, A., Werring, D., Chen, C., Smith, C., van Buchem, M., Norrving, B., Gorelick, P.B., Dichgans, M., nEuroimaging, S.T.f.R.V.c.o., 2013b. Neuroimaging standards for research into small vessel disease and its contribution to ageing and neurodegeneration. *Lancet Neurol.* 12, 822–838.
- Willie, C.K., Colino, F.L., Bailey, D.M., Tzeng, Y.C., Binsted, G., Jones, L.W., Haykowsky, M.J., Bellapart, J., Ogooh, S., Smith, K.J., Smirl, J.D., Day, T.A., Lucas, S.J., Eller, L.K., Ainslie, P.N., 2011. Utility of transcranial Doppler ultrasound for the integrative assessment of cerebrovascular function. *J. Neurosci. Methods* 196, 221–237.
- Wise, R.G., Pattinson, K.T., Bulte, D.P., Chiarelli, P.A., Mayhew, S.D., Balanos, G.M., O'Connor, D.F., Pragnell, T.R., Robbins, P.A., Tracey, I., Jezzard, P., 2007. Dynamic forcing of end-tidal carbon dioxide and oxygen applied to functional magnetic resonance imaging. *J. Cereb. Blood Flow. Metab.* 27, 1521–1532.
- Wong, E.C., 2007. Vessel-encoded arterial spin-labeling using pseudocontinuous tagging. *Magn. Reson Med.* 58, 1086–1091.
- Yezhuvath, U.S., Lewis-Amezua, K., Varghese, R., Xiao, G., Lu, H., 2009. On the assessment of cerebrovascular reactivity using hypercapnia BOLD MRI. *NMR Biomed.* 22, 779–786.
- Yoon, S., Zuccarello, M., Rapoport, R.M., 2012. pCO(2) and pH regulation of cerebral blood flow. *Front. Physiol.* 3, 365.
- Yun, T.J., Paeng, J.C., Sohn, C.H., Kim, J.E., Kang, H.S., Yoon, B.W., Choi, S.H., Kim, J.H., Lee, H.Y., Han, M.H., Zaharchuk, G., 2015. Monitoring cerebrovascular reactivity through the use of arterial spin labeling in patients with moyamoya disease. *Radiology* 278, 205–213.
- Zaidat, O.O., Fitzsimmons, B.F., Woodward, B.K., Wang, Z., Killer-Oberpfalzer, M., Wakhloo, A., Gupta, R., Kirshner, H., Megerian, J.T., Lesko, J., Pitzer, P., Ramos, J., Castonguay, A.C., Barnwell, S., Smith, W.S., Gress, D.R., Investigators, V.T., 2015. Effect of a balloon-expandable intracranial stent vs medical therapy on risk of stroke in patients with symptomatic intracranial stenosis: the VISSIT randomized clinical trial. *JAMA* 313, 1240–1248.